PlasticFreeDanube

3D HYDRODYNAMIC FLOW MODELS

Report

DOCUMENT INFORMATION	
Work Package	3 Material Flow and Transport Modelling
Activity	3.6 3D hydrodynamic modelling of selected plastic accumulation zones
Detailoutput	3.6.1 3D hydrodynamic flow models

Version	Date	Author/s	Organisation
v.1.0	30/03/2021	Marcel Liedermann, Sebastian Pessenlehner, Michael Krapesch, Dorian Shire, Sabrina Schwarz, Philipp Gmeiner, Ferdinand Bakanic	BOKU

Inhaltsverzeichnis

1. Introduction 3
2. Project area 3
   2.1. Modelling reaches 4
      2.1.1. 3D model – Haslau-Regelsbrunn 4
      2.1.1. 3D model – Wildungsmauer-Witzelsdorf 5
      2.1.2. 3D concept model 6
      2.1.1. 2D model – Vienna-Bratislava 6
3. Basics 7
   3.1. Engineering structures 7
      3.1.1. Guiding walls 7
      3.1.1. Groynes 7
   3.2. Plastics 10
      3.2.1. Definition and delineation 10
      3.2.1. Density 10
      3.2.2. Degradation 11
      3.2.3. Input and exit pathways of macroplastics 11
      3.2.4. Plastic measurements 12
      3.2.5. Environmental impact of macroplastics 12
   3.3. Numerical modelling 12
   3.4. RSim 13
      3.4.1. RSim 2D 13
      3.4.2. RSim 3D 13
4. Methodology 14
   4.1. Digital terrain model 14
   4.2. Computational mesh 17
      4.2.1. Boundary conditions 19
   4.3. Calibration and validation 20
   4.4. Hydrology 23
   4.5. Quantification of macro plastic accumulation potential 24
      4.5.1. Bank near accumulation zones 25
      4.5.1. Floodplain accumulation zones 27
5. Results 27
   5.1. 3D numerical models 27
      5.1.1. 3D model Haslau-Regelsbrunn 27
      5.1.2. 3D model Wildungsmauer-Witzelsdorf 33
      5.1.3. 3D concept model 35

5.2. 2D numerical model 40
5.2.1. Flow velocity 40
5.2.2. Water depth 41
5.2.3. Water levels 42
5.2.4. Bank-near accumulation zones 43
5.2.5. Floodplain accumulation 49
6. Summary and Conclusiones 55
7. Directories 57
7.1. List of figures 57
7.2. List of tables 58
8. References 59

1. Introduction

One of the objectives of the project „PlasticFreeDanube“ is an analysis of the main sources, inputs and pathways of plastic waste in the Danube and on its river banks. Within the current activity 3.6 "3D hydrodynamic modelling of selected plastic accumulation zones” it is aimed to describe fluvial processes related to plastic waste in river systems by the means of numerical simulation. The areas selected for the investigation were defined according to the findings of activity 3.5 “Map of plastic accumulation zones”, where typical plastic accumulation zones were evaluated according to hydromorphological aspects.

In a first step digital terrain models (DTM) of the riverbed were created as a basis for the hydraulic simulation in order to build up a numerical model. The applied 3D flow simulation model RSim-3D (Tritthart, 2005) is based on the "Finite Volume Method". The spatial discretization is done by an unstructured computational mesh of polyhedral cells. Based on the depth-averaged Reynolds equations, numerical solutions are iterated using the SIMPLE algorithm to calculate the pressure correction. Turbulence calculation is performed using a k-ε model. The free surface is calculated iteratively by continuously determining the water surface based on the pressure field in the cells near the surface. In this process, the model must be calibrated and validated using measurement data collected in the field, such as flow velocities, discharges and water levels. To do this, several field measurements were conducted. Different flows (e.g. mean water and 1-year flood event) were used to represent the naturally prevailing flow conditions.

The resulting 3D information of flow velocities and flow directions, bed shear stresses, partial flows and water level positions for different discharge conditions were basically plotted in maps and used for further analysis.

2. Project area

The study area related to numerical modelling covers the eastern Austrian section of the Danube, starting from Vienna to the Slovakian border. The Austrian Danube has an average gradient of about 0.4° (40 centimeters per kilometer). The average flow velocity varies between 1 and 3 meters per second. Floods caused by snowmelt are characteristic for this river mainly from late spring to the summer months, while floods due to precipitation events can occur all year round (Nationalpark Donau-Auen, 2017). Major regulation measures on the Danube took place in the 19th century, mainly to meet the requirements of inland navigation. Since then, the mainstream at many sections of the Danube, as also in the present study area, has been characterized by engineering structures such as groynes and guiding structures. At the same time, adjacent side arms have been successively cut off. The surrounding foreland of the considered Danube section is also a national park area, which consists mainly of floodplain forests and meadows and is administered by the Nationalpark Donau-Auen. The total length of the Danube River in Austria is about 350 kilometers, of which about 36 kilometers are flowing through the area of the national park. The main tributaries in the National Park are as follows: Schwechat, Fischa, Rußbach and March/Thaya. (Nationalpark Donau-Auen, 2017).

Based on the derived findings – as described in deliverable D 3.5.1 “Map of plastic accumulation zones” - from site visits, available data from experts of the Nationalpark Donau-Auen and a GIS-based hydromorphological analysis, reaches for 2D and 3D numerical simulation were defined as depicted in Figure 1. The modelling reaches cover:

- 3D model Haslau-Regelsbrunn: river-kilometer 1901 - 1903,5
- 3D model Haslau-Wildungsmauer-Witzelsdorf: river-kilometer 1903,5 1891,7 - 1895,2
- 2D model Vienna-Bratislava: river-kilometer 1907 - 1881,3
- 3D concept model

Figure 1 shows the defined model boundaries and the respective dimensions of the model. Detailed information on the location and dimensions of the concrete models can be found in the following subchapters.

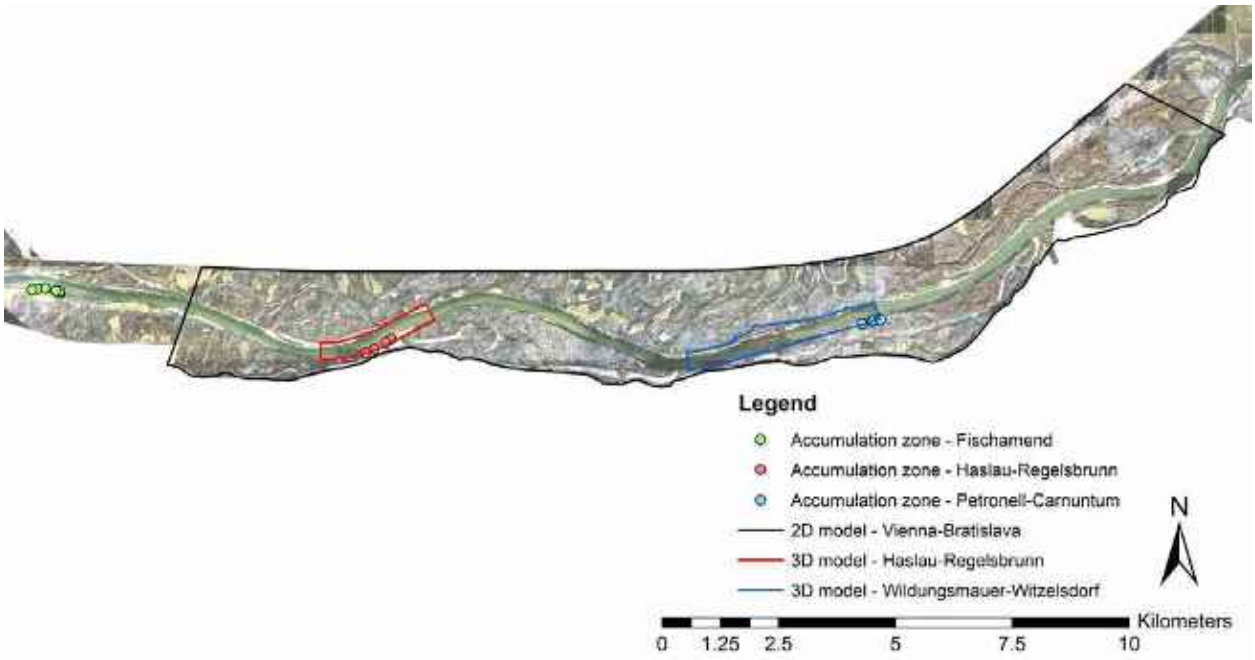


Figure 1 Defined modelling reaches for 2D and 3D numerical simulation based on accumulation zones detected during site visits, expertise from Nationalpark Donau-Auen and GIS-bases analysis of the hydraulic structures of the Danube River

2.1. Modelling reaches

2.1.1. 3D model – Haslau-Regelsbrunn

The first project area was defined near Haslau-Regelsbrunn between stream-km 1901 and 1903.5, since the assumption of accumulation zones on the right shallow bank of the Danube corresponds well with both field samplings and experience of the Nationalpark Donau-Auen. The area to be modelled thus covers a reach of 2.5 km of the Danube. In this section, the Danube flows towards the north-east and further follows a straight course between river kilometer 1902.5 and 1901.

A guiding wall, as well as several groyne fields are located at the outer bend of the river, with the guiding wall directing the flow towards the left bank. In addition, the groynes present in the project area are orthogonal groynes made of riprap stones. Clear deposition trends are evident both in and downstream of the groyne fields. In order to be able to describe the flow field with sufficient accuracy in comparison with the natural state (mapping of secondary flows, flow velocities and directions in different depth layers, etc.), a three-dimensional model was set up (Tritthart, 2017).

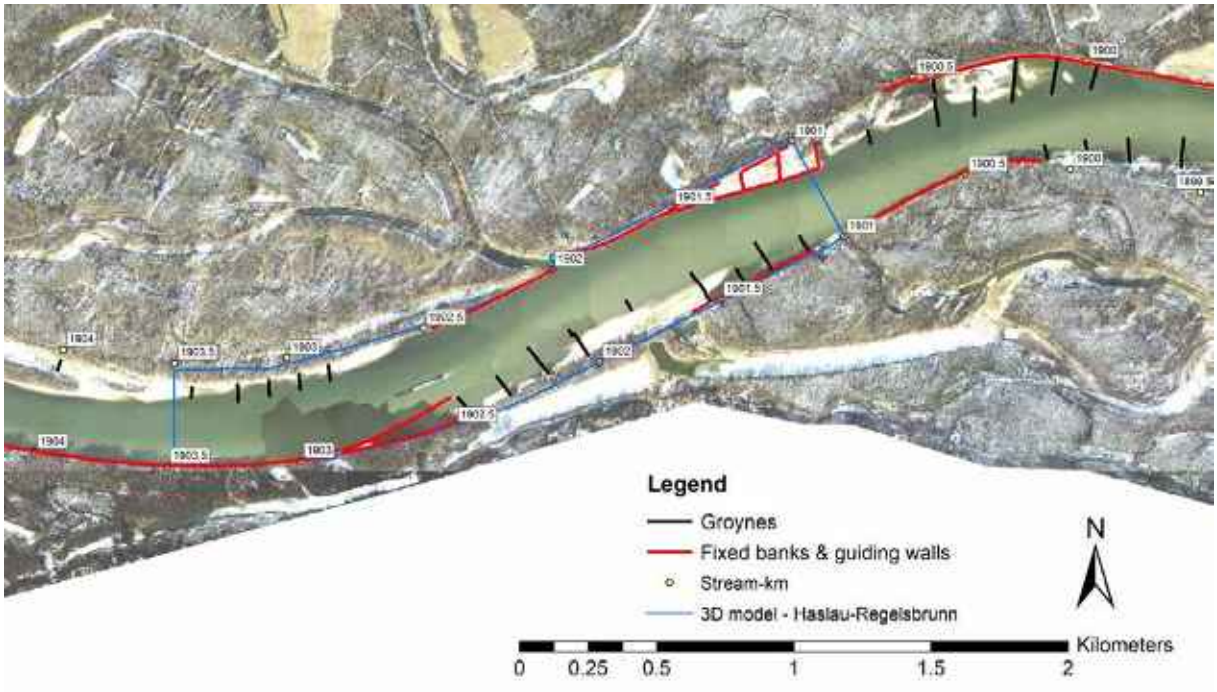


Figure 2 Model reach - 3D numerical model – Haslau-Regelsbrunn

2.1.1. 3D model – Wildungsmauer-Witzelsdorf

The second model reach is located near Wildungsmauer-Witzelsdorf covering a section of 4.2 km from stream-km 1891 to 1895.2 and was defined primarily because of the high amount of macro plastic found by volunteers during sampling actions.

Looking at Figure 3, several orthogonal groynes are visible on the left bank of the river between river kilometre 1895.2 and 1894. The orthophoto also shows that sedimentation has already progressed between the groyne fields. In addition, a guide structure on the left bank leads the current towards the main channel. Downstream of the guiding wall, a groyne field with declined layout is to be found. On the right bank of the river, there are further noteworthy orthogonal groynes downstream from river kilometre 1892.

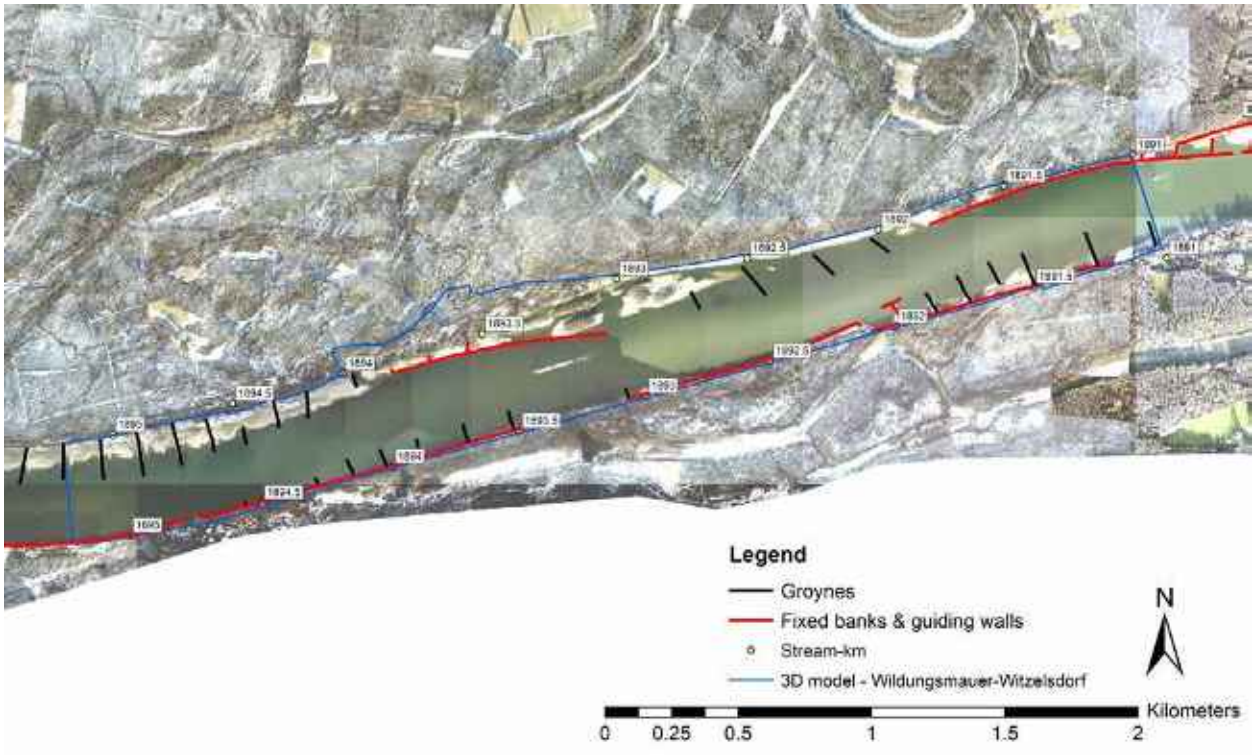


Figure 3 Model reach - 3D numerical model – Wildungsmauer-Witzelsdorf

2.1.2. 3D concept model

For the selection of a schematic concept model an attempt was made to obtain the best possible representativeness for the Danube River east of Vienna. The choice subsequently fell on a 7 km long area near Haslau-Regelsbrunn from stream-km 1898 to 1905. Another advantage of relating the schematic model to a real section of the Danube is the possibility to compare the schematic channels created with the current state model near Haslau-Regelsbrunn to obtain new insights.

2.1.1. 2D model – Vienna-Bratislava

The area of the 2D model covers the distance from stream-km 1907 to 1881.3 and thus includes almost the entire Danube section from Vienna to Bratislava (Glock, 2018). The exact model boundaries can be seen in Figure 4. As described earlier, the Danube east of Vienna is surrounded by the Danube floodplains. While in the south the boundary of the Nationalpark Donau-Auen results from geology (break-off edge of the Vienna Basin), the northern boundary is formed by flood protection dam built in the 19th century (Nationalpark Donau-Auen, 2017). According to these natural and anthropogenic boundaries, the southern and northern model boundaries resulted, respectively. Engineering structures in the main channel, as well as separated side arms are included in the model.

Besides a large-scale analysis of diversion of macro plastic to the side channels and floodplain areas during flood events, this large-scale model also intended to provide information about accumulation zones in morphological depressions using particle tracking. This can be visualized by a "bathtub effect" during flood events. After the peak of a flood event the flow is subsequently reduced and the water level in the foreshore successively decreases correspondingly. In the end, water remains in depressions where, due to the elevation gradient, it can no longer flow out but can only evaporate or percolate into the soil, resulting in the deposition of the macro plastic located in the depression as observed in field sampling actions.

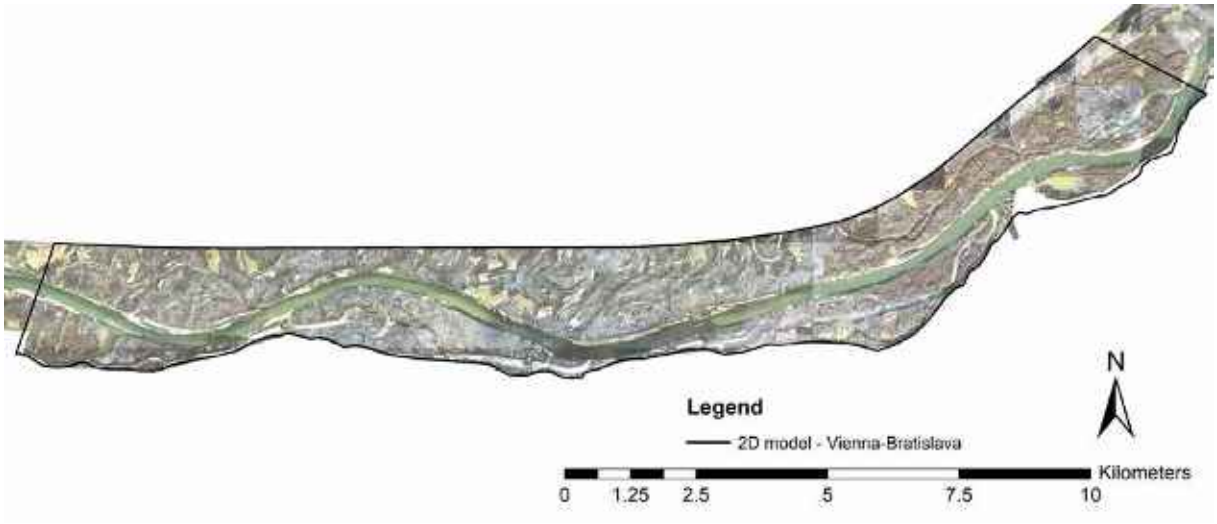


Figure 4 Model reach - 2D numerical model – Vienna-Bratislava

3. Basics

3.1. Engineering structures

3.1.1. Guiding walls

Guiding walls are longitudinal dam-like structures that can usually be submerged and whose primary function is to guide the direction of water flow. Usually they are installed on one side of particularly endangered outer banks, with flow cross-sections being constricted almost parallel to the current. This increases the bottom shear stress in the cross-section and consequently the bed erosion. The height of guiding walls is usually related to mean water level. The construction of guiding walls also often proves to be very difficult due to the high flow velocities and large water depths immediately upstream of the structures (Nachtnebel, 2008).

3.1.1. Groynes

The groyne field represents the area between two successive groynes, the remaining river tube and the river bank. The length of the groyne field is understood to be the distance between two successive groynes (Malcherek, 2014). The design height of groynes usually is related to low water level, in order to tackle the problem of shallow fairway depths for navigation occurring during low flow conditions.

Classification of groynes can be done, for example, according to their construction material. Construction materials include stones, rootstocks, wattle, and stone box groynes. Structural repairs or modifications of groynes can also be easily done afterwards (Patt et al., 2011). According to their orientation in the river channel (Figure 5), groynes are divided into:

- Declinant / downstream
- Inclinant / upstream
- Right-angled/ orthogonal

Inclined groynes serve as good bank protection, but lead to high sedimentation of solids behind the groynes. The situation is different for declined groynes, where both bank protection and the sedimentation rate are relatively low. Orthogonal groynes, like inclined ones, result in high siltation downstream of the groynes (Patt et al., 2011).

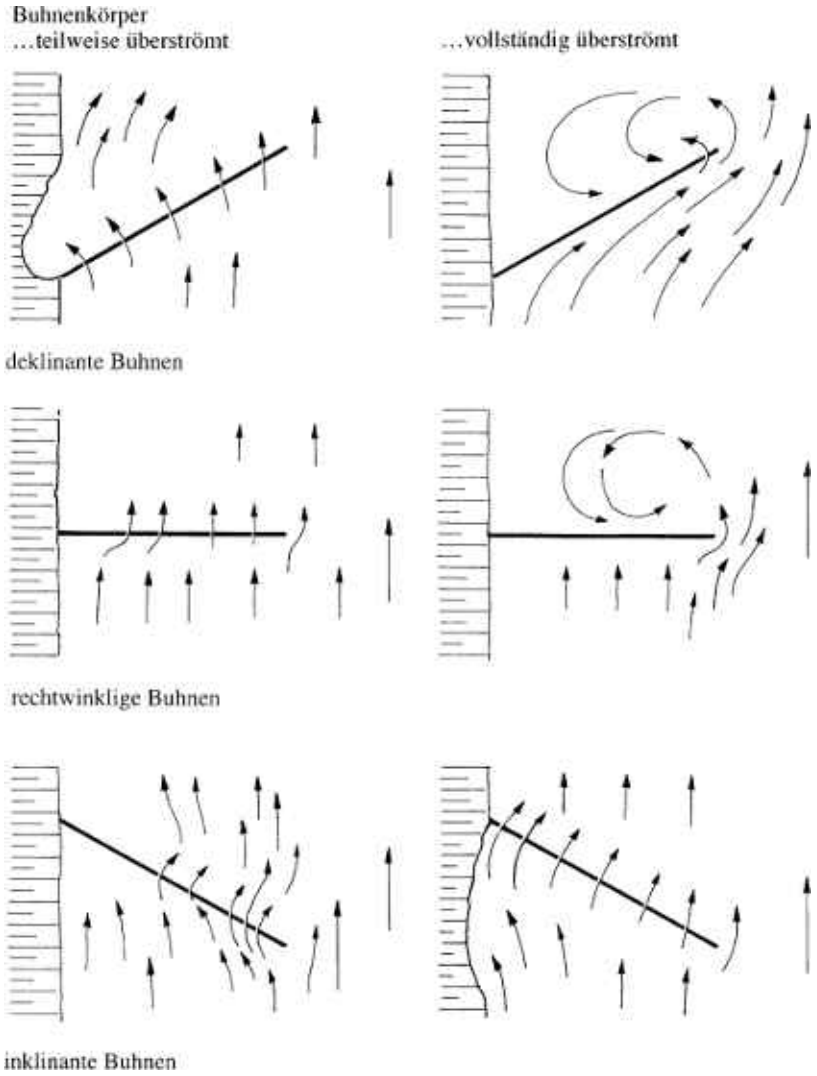


Figure 5 Construction methods and associated flow patterns of groynes (Patt et al., 2011)

3.1.1.1. Groyne induced flow fields

Vortex formation

Sukhodolov et al. (2002) recognized that vortex formation in groyne fields depends primarily on the ratio between groyne length and groyne spacing. The ratio thus has a strong influence on the location and number of vortices that form, resulting in a wide variety of flow patterns in groyne fields with different ratios. Looking at the left sketch in Figure 6, the distance between the groynes is so small (Lg/Lf>2.0) that two eddies form next to each other. Thus, there is hardly any movement of the water body in the groyne field, due to a low momentum exchange between the two eddies. While only one vortex is formed at a ratio of 0.5<Lg/Lf<2.0, a secondary vortex (upstream) and a primary vortex (downstream) are already formed at a ratio of Lg/Lf<0.5 (Sukhodolov et al., 2002).

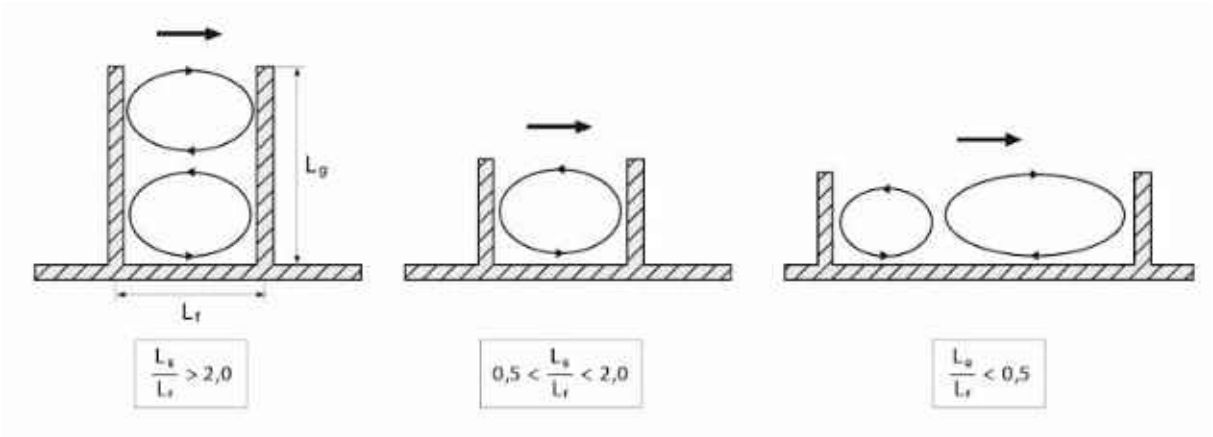


Figure 6 Vortex formation in groyne field as a function of geometry (Sukhodolov et al., 2002)

Flow around groyne structure

A groyne effect, as previously described, is the concentration of flow to the center of the channel by constriction of the flow cross-section. This phenomenon occurs when water is flowing around the groyne at low discharge conditions. Downstream of the groyne, however, the cross-section widens again, resulting in backflow. According to the groyne spacing, a circulation flow develops from this reverse flow, caused by an impulse release of the primary flow (Figure 7). Due to the primary circular currents, secondary circular currents (corner vortices) can be partially driven again in the corners at the groyne roots (Malcherek, 2014). Since the velocities of the circular currents in the groyne field are lower than in the river bed, solids are deposited in the groyne field. Near the groyne heads, local depressions, so-called scour holes, often occur due to strong turbulent currents. (Nachtnebel, 2008)

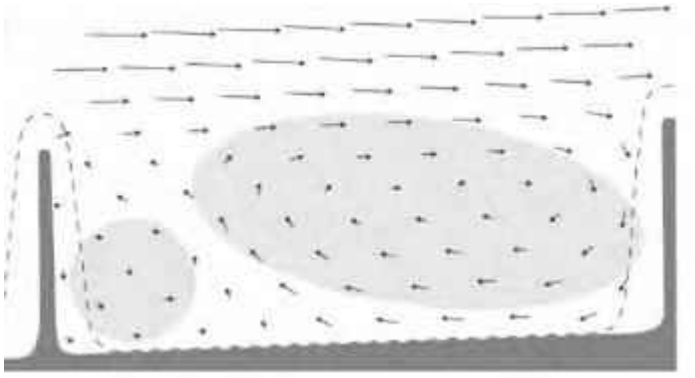


Figure 7 Velocity distribution and vortex formation during flow around a groyne (Schnauder et al., 2015)

Submerged groyne

If the groyne is submerged, an eddy with a horizontal axis parallel to the groyne is created behind the groyne, which simultaneously results in a complex flow condition. If the groyne is significantly overflowed, flow velocities and directions in the groyne field are expected to be similar to those in the river channel (Figure 8). This may then be followed by further mobilization of the already deposited solids. Depending on the orientation of the groyne, the flow is thereby directed towards the centre of the river (inclinant groyne) or the river bank (declinant groyne). (Nachtnebel, 2008)

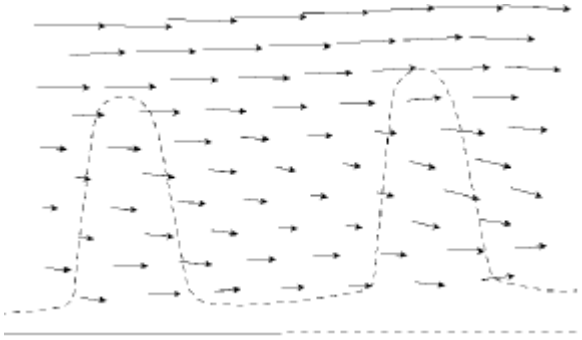


Figure 8 Near-surface velocity vectors during overflow of a groyne (Schnauder et al., 2015)

Maximum bed shear stress

As field experiments by Schnauder et al. (2015) show, the maximum bed shear stresses occur in the area of flow separation at the groyne heads, and thus coincide with the largest velocity gradients. There is little difference in the magnitude of the maximum values of over- and surrounding flow, while notable differences are seen within the groyne field. In the case of overflow, a local maximum is recorded behind the groyne, which is due to the strong turbulence production in the shear layer of the vertical detachment at the groyne crest.

3.2. Plastics

3.2.1. Definition and delineation

An international standard for a size classification of plastics does currently not exist (Hohenblum et. al., 2015). International expert groups (GESAMP, 2015) set the boundary between micro- and macro plastics at a particle diameter of 5 mm, as does the relevant literature (Arthur et al., 2008). The 2013 Monitoring Guidance for Marine Litter in European Seas from the Marine Strategy Framework Directive (MSFD) Working Group on Marine Litter makes the following more precise plastic classification based on particle size:

- >25 mm macroplastic
- 5 - 25 mm mesoplastic
- 1 - 5 mm large microplastic particles
- < 1 mm small microplastic particles

With this classification of the MSFD (2013), a classification valid throughout Europe is proposed. A further distinction is made between primary and secondary micro plastic. While primary micro plastic is already produced as such for various products in industry, secondary micro plastic is formed by the chemical or physical degradation of macro plastic by UV radiation and wave impact (Arthur et al., 2008).

3.2.1. Density

Probably the most important property of plastic is its density, as this has a significant influence on its movement in water. Depending on the particular starting material, the density of plastic varies by about 1.0 g/cm³ and it can therefore migrate differently in the water. Lighter plastic particles tend to float on the surface, while heavier particles sink towards the bottom of the water. The surface-to-volume ratio is also decisive for the behaviour of the particle in the water. Particles with a low ratio sink or float faster, while particles with a high ratio move predominantly in suspension, depending on the turbulence. Since rivers always exhibit turbulence, it can be assumed that a not inconsiderable proportion of the total macro plastic in the water body is also transported within the water column. In particular, plastic films tend to move in suspension within the water column, while plastic parts such as bottle

caps tend to be found at the water surface (Tweehuysen, 2015). Biofouling also affects the density of plastic. A biofilm can form on the surface of the plastic particle, which is mainly populated by algae. Subsequently, this increases the density of the plastic, causing it to sink in the water. (Long et al., 2015; Kowalski et al., 2016; Harrison et al., 2018).

3.2.2. Degradation

Andrady (2011) distinguishes between the following influences or occurring reactions, which significantly affect the degradation process of plastics:

- biological (degradation by microbes)
- photochemical (UV-induced reaction)
- thermal (reactions caused by temperatures, including thermo-oxidation)
- hydrolysis (reaction with water)

While the influence of biological degradation, hydrolysis and thermal oxidation can be considered minor, it is mainly the photochemical reaction induced by UV radiation that should be understood as an important degradation process of plastic. The lifetime of plastics in nature varies not only due to the prevailing degradation processes, but also depends on the particular plastic material. Furthermore, it is essential whether the plastic is floating in the water or is already stranded. This also influences the degradation process, as it takes place faster on land than in water. (Andrady, 2011)

3.2.3. Input and exit pathways of macroplastics

Input pathways

Breitbarth (2017) divides direct and indirect input pathways of macrowaste into streams. Sources of direct input pathways include smaller water bodies that flow into a river section. Other sources include illegal waste disposal, wastewater treatment plants, rainwater overflows and littering (Breitbarth, 2017). The share of macro waste, which is discharged into the Danube via wastewater treatment plants, is probably to be classified as relatively low due to the mechanical treatment process. The Vienna sewer network consists of several collector sewers, some of which have a separation and combined system and finally discharge the wastewater into the main treatment plant in Simmering. By means of measures such as the completion of the main collector sewer in 2000, peak discharges became more manageable. This reduced the need to discharge sewage water via overflows into the watercourse during extreme precipitation events (Stadt Wien, 2018). Despite such fundamental improvements, it can still be assumed that a significant proportion of macroplastics enters the Danube via rainwater overflows. Another pathway of macroplastics into the Danube that should not be underestimated is the so-called littering. Another indirect pathway is the careless disposal of waste along the riverbanks (Breitbarth, 2017). Heeb and Hoffelner (2004) define littering as the careless discarding of waste at its point of origin in public spaces without using the disposal facilities provided for this purpose - not to be confused with illegal disposal of household waste to avoid disposal fees. PET bottles, plastic packaging, and plastic shopping bags are considered common littering items. Since there are many shallow shoreline areas in the National Park area that are used for recreational purposes and other purposes, littering of macroplastics, especially PET bottles, through the water banks cannot be ruled out.

Exit pathways

A large proportion of macroplastic debris is washed onto the banks of watercourses. This is shown above all by findings in the area of the Nationalpark Donau-Auen, but studies in Germany such as that of Breitbarth (2017) also provide evidence of this phenomenon. Floods in particular ensure that plastic also reaches further into the forelands,

where the plastic waste is deposited in depressions. In addition, grates at hydropower plants retain a not inconsiderable amount of macroplastics.

3.2.4. Plastic measurements

Microplastics

The IWA of the University of Natural Resources and Applied Life Sciences modified a bedload sampler (BfG sampler) to perform measurements of microplastic particles in the Danube River. The sampler consists of three frames to perform measurements at the water surface, in a deep layer and near the river bottom. The lowest rectangular steel frame has side lengths of 30x60 cm and is covered with a 500 µm mesh. Two steel double frames with inlet openings measuring 60x60 cm are also attached at different heights. One net on one side of the double frame has a mesh size of 500 µm, while the other net has a mesh size of 250 µm. (Liedermann et al., 2018)

Macroplastics

One method for the detection of macroplastic particles in water bodies is, for example, the "WFW Sampler MK-I", which has been specially adapted for use on rivers (Figure 21). This measuring device was developed by the organization Waste Free Waters and detects plastic particles with the help of two metal nets both at the water surface and within the water column. The instrument can be towed either alongside or behind a boat. Measurements have been carried out on the Maas (Netherlands), the Rhine (Netherlands) and the Danube (Romania). A mesh size of the net of 3.2 mm has proven itself, since smaller mesh sizes led to a faster clogging of the nets. (Tweehuysen, 2015)

3.2.5. Environmental impact of macroplastics

If plastic is not disposed of appropriately and enters the environment through a discharge pathway, this has both ecological and economic impacts (Breitbarth, 2017). Due to UV radiation from the sun, as well as mechanical impacts such as wave action, plastic in water becomes brittle after prolonged exposure. This causes the plastic to slowly dissolve into smaller fragments (microplastic < 5 mm). However, these microparticles cannot be biodegraded by microorganisms. Subsequently, the particles can be swallowed by fish, which may misinterpret microplastics as food (Browne et al., 2007). Furthermore, aesthetic aspects have to be considered, as the Danube Floodplain National Park with its Danube banks and surrounding floodplain forests is used as a recreational area. Pollution of the environment would significantly deteriorate both the landscape and the recreational value. Voluntary collection activities are currently taking place in the Nationalpark Donau-Auen to counteract increasing pollution of the environment by plastic (Nationalpark Donau-Auen, 2018).

Last but not least, technical structures such as locks, weirs and dams are also affected by plastic accumulation. Upstream of the turbine inlet of hydropower plants, grates are installed in all types of power plants to keep debris away from the turbine. The bar spacing is between 50 - 100 mm for coarse rakes and between 20 - 30 mm for fine rakes. The debris retained by the rake can then be disposed. In many cases, however, plastic waste also accumulates, which results in time-consuming and cost-intensive manual separation (Giesecke, 2014). However, flushing and flushing devices at hydropower plants only carry the problem on to another location, until finally a discharge into the oceans takes place. The result is, among other things, the formation of so-called big garbage patch. (Breitbarth, 2017)

3.3. Numerical modelling

A numerical model attempts to represent hydraulic processes and properties as best as possible with the aid of computational simulation. Numerical algorithms are used to solve the underlying physical equation systems (Strobl & Zunic, 2006). Hydrodynamic problems always refer to a model domain in space and time, covered by a network

of computational points, where the model provides results for the desired hydrodynamic variables at each of these points. The time period of the simulation is discretized by individual time steps and the structure of the spatial grid can be one, two or three dimensional (Malcherek, 2014). By means of application of numerical models, almost all areas of the water cycle can be simulated nowadays, such as flood simulations, the verification of flow conditions in water bodies to secure navigation or the extraction of drinking water. In this context, models can be used in the planning of new hydraulic engineering measures, assessment of existing situations, or for the reconstruction of events, as is the case in the present work (Forkel, 2004). Compared to physical models, numerical models have advantages mainly due to their faster, less expensive creation and adaptation, but also due to the absence of scale effects and the possibility of almost unlimited size of the model. While physical models require longer construction times, numerical models often exhibit long computation times. However, due to the continuous optimization of computational capacities, the use of numerical models is increasing (Strobl & Zunic, 2006).

Within activity 3.6. - "Hydrodynamic modelling of selected plastic accumulation zones" it is aimed to set up 2D and 3D numerical models in order to describe and analyse the hydrodynamic characteristics of defined accumulation zones in the project areas. The used software is RSim (Tritthart, 2017).

3.4. RSim

This chapter is dedicated to the applied software packages, which are used for the numerical determination of flow characteristics in streams. Furthermore, the application of particle tracking in RSim is explained in more detail, since this function provides an essential contribution to the hydraulic characterization of the accumulation zones.

Both RSim-2D and RSim-3D distinguish between the pre-processing mode for data preparation and the post-processing mode for visualization of the simulation results. These steps are performed with the graphical user interface, called RSim-GUI.

3.4.1. RSim 2D

The RSim-2D software package was developed by Michael Tritthart in 2008 - 2009 (Tritthart, 2017). RSim-2D uses an unstructured computational mesh based on triangular cells. The finite element method (FEM) is applied to solve the flow equations. Furthermore, the Smagorinsky model is applied for turbulence modeling and a 1^{st} or 2^{nd} order explicit method is applied for time discretization at the user's choice. The following input data are required for 2D modelling (Tritthart, 2017):

- Terrain model
- break lines
- roughness values
- flow (steady-state) or flow hydrograph (non-stationary) at the inflow boundary
- water level at the outflow boundary

3.4.2. RSim 3D

The software package "River Simulation in 3D", RSim-3D for short, was developed by Tritthart (2006) and has been continuously revised since 2005. Unlike the 2D model, RSim-3D uses a three-dimensional unstructured computational grid, which is created from a 2D Voronoi decomposition of the flow field and a vertically structured subdivision of the continuum. The computational grid is constructed based on cells with arbitrary, predominantly hexagonal planforms (Tritthart, 2006). In RSim-3D, the Reynolds-averaged Navier-Stokes equations are solved numerically using finite volume method (FVM). Basically, steady-state and unsteady-state flows are possible for the calculation, whereas the computational effort for unsteady-state flows is considerably higher. For turbulence modelling the k-ε model is applied and for time discretization an implicit 1st order method is used. The required

input data for the model are the same as those for 2D modelling, with an additional water level pre-estimation required. (Tritthart, 2017)

4. Methodology

4.1. Digital terrain model

The used digital terrain model covering the Danube from Vienna to Bratislava - stream-km 1907 to 1881.3 - is based on terrain data collected using different measurement methods. On the land side, the information regarding the position and elevation of the terrain points comes from a laser scan, while below the water level, the data was recorded with single-beam and multi-beam measurements. The point information of the terrain model is arranged in a grid and has a resolution of 2 x 2 m. (Tritthart & Glock, 2018). The terrain models Vienna-Bratislava, Haslau-Regelsbrunn and Wildungsmauer-Witzelsdorf are depicted in Figure 9; a detailed overview of the used data is given below:

- Lasers can (May 2010)
- Single-Beam (February 2010)
- Single-Beam (October 2015)
- Multi-Beam (June 2010)

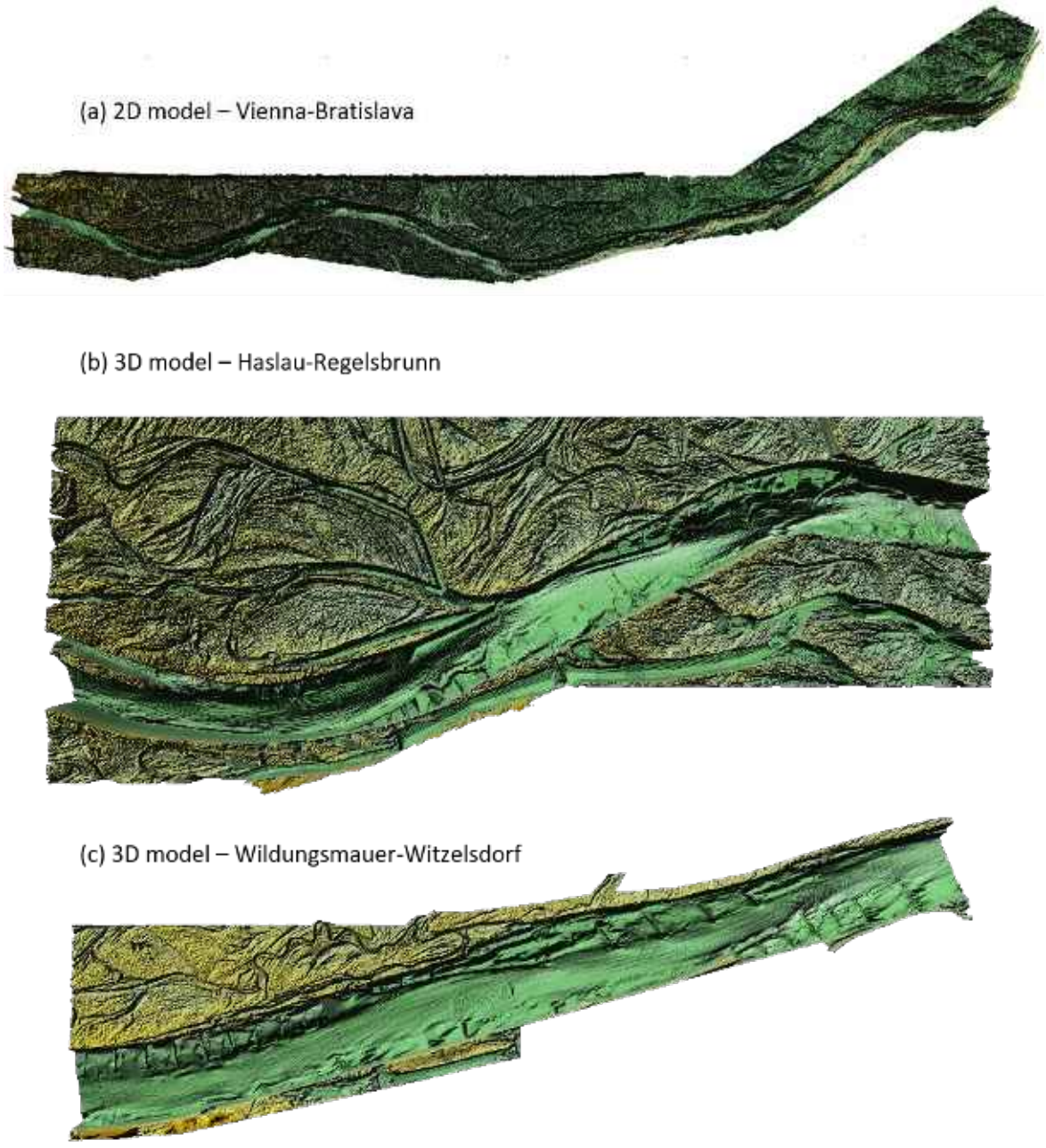


Figure 9 Digital Terrain Models – (a) Vienna-Bratislava, (b) Haslau-Regelsbrunn and (c) Wildungsmauer-Witzelsdorf

For the schematic concept model, a total of 70 profiles with a spacing of 100 m each were selected from the existing terrain model. The selected profiles were statistically analysed using the LOESS method (locally weighted scatterplot smoothing), which is a very widely used smoothing method using a locally weighted regression function. This method was chosen because outliers are weighted less than in other methods. (Fahrmeir et al., 2009). By applying this data analysis, a very simplified model using a plane bed (model 1) as well as model more related to natural bed evolution with inner and outer band sequences (model 2) were developed (see Figure 10). Figure 11 shows the concept model with integrated groynes, both for model 1 with plane bed and model 2 with inner and outer bed sequences.

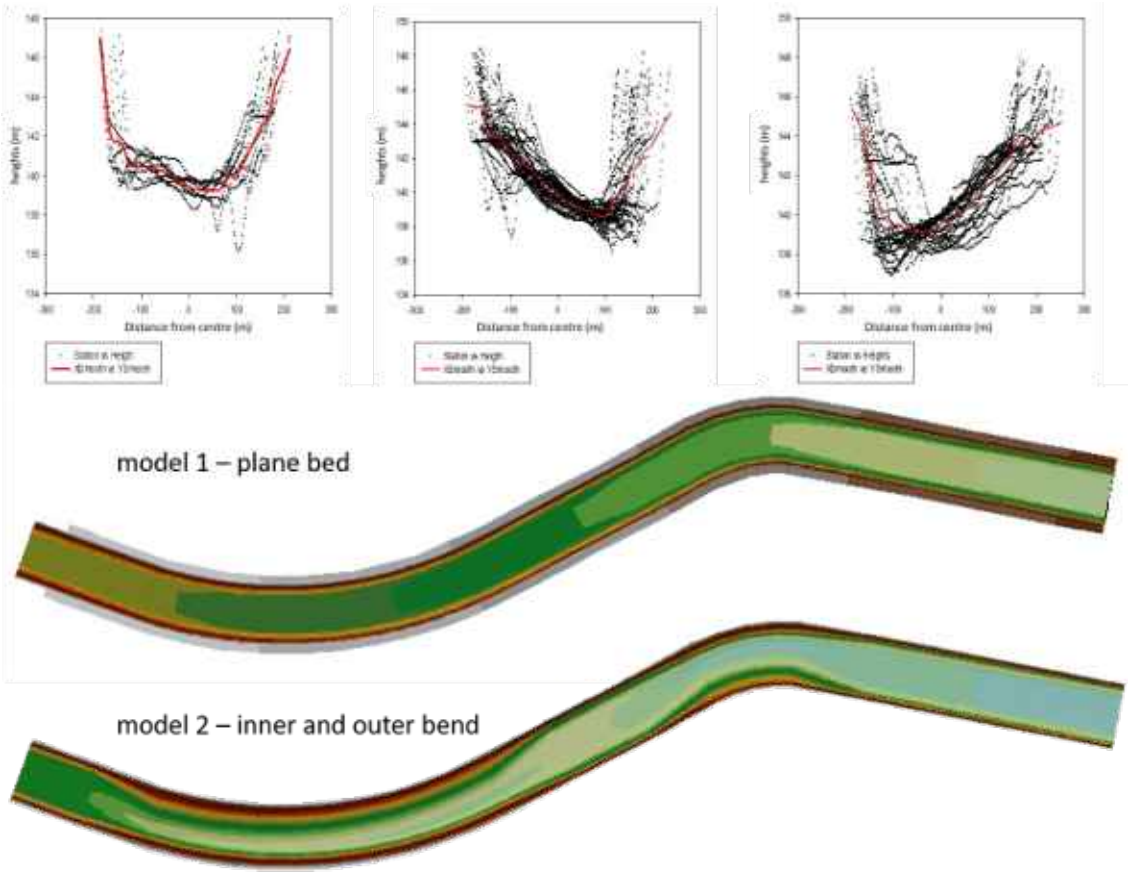


Figure 10 Terrain data analysis and resulting digital terrain models for the concept model - mode1: plane bed; model 2: inner and outer bed sequences

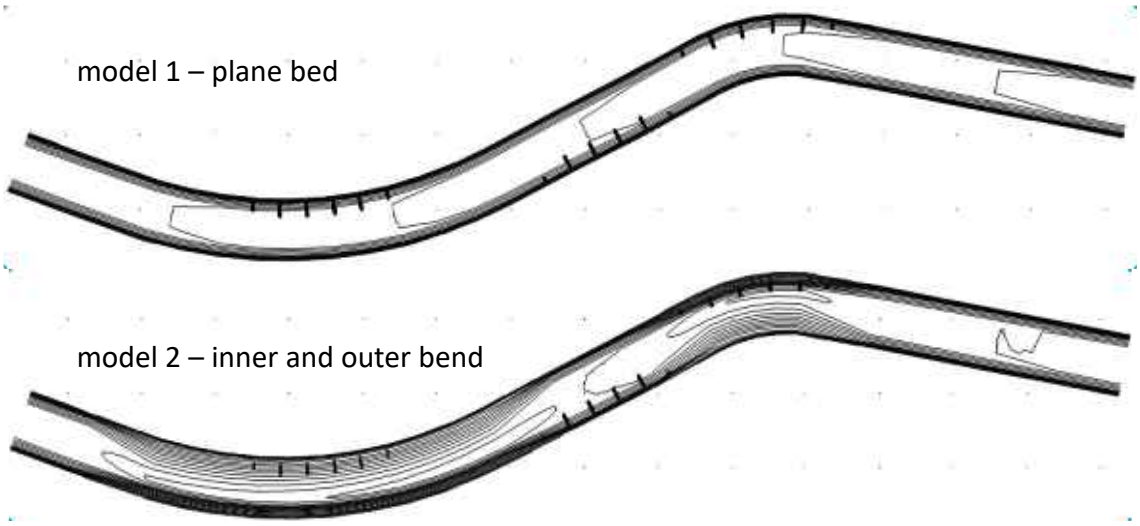


Figure 11 Concept model with integrated groynes - mode1: plane bed; model 2: inner and outer bed sequences

Furhtermore a third concept model in order to evaluate single groyne effects was introduced based on the same geometry as model 2. However, this model only contains one single groyne in the first left bank groyne field.

4.2. Computational mesh

In order to build up a computational mesh in RSim-GUI, a digital terrain model is used as a data basis. The boundary of the model area is defined by a boundary polygon, while structural polygons are used to generate different distances of computation points. The generation of computation points is done by regular distances to each other or in predefined normal distances to the polygon. Since with a smaller distance between the computational points a larger computational accuracy accompanies, it makes sense to provide the investigation area with different zones of point distances. This shortens, among other things, the calculation time and results can be output faster. To avoid an abrupt change from smaller to larger cells, additional intermediate points (transition zones) must be generated.

Subsequently, the computational mesh for RSim-3D is generated from primarily hexagonal computational cells by means of the mesh generator implemented in RSim-GUI. The computational mesh in RSim-2D, unlike in RSim-3D, consists of triangular cells rather than hexagonal cells. Furthermore, the terrain coordinates are transferred to the computational mesh, whereby an interpolation (Kriging procedure) is necessary, since the grid of the computational mesh does not correspond to that of the terrain model. An example of a final computational mesh for the 3D model Haslau-Regelsbrunn is given in Figure 12, a detail providing the transition zones for finer and coarser cell sizes is depicted in Figure 13, while Figure 14 contains the mesh for the 2D model Vienna-Bratislava.

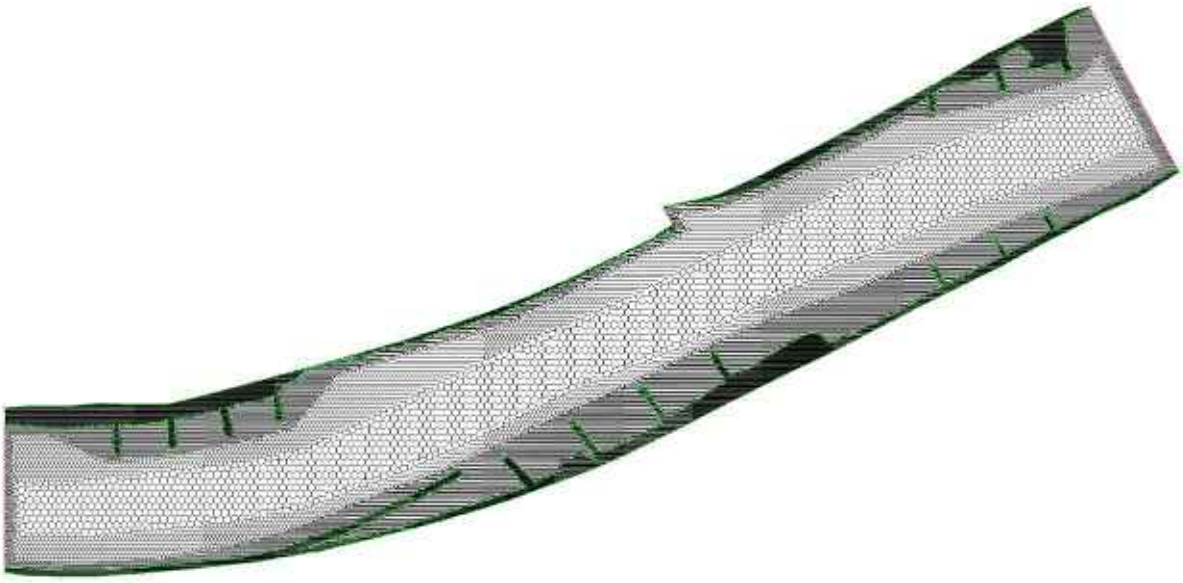


Figure 12 Computational mesh - 3D model Haslau-Regelsbrunn

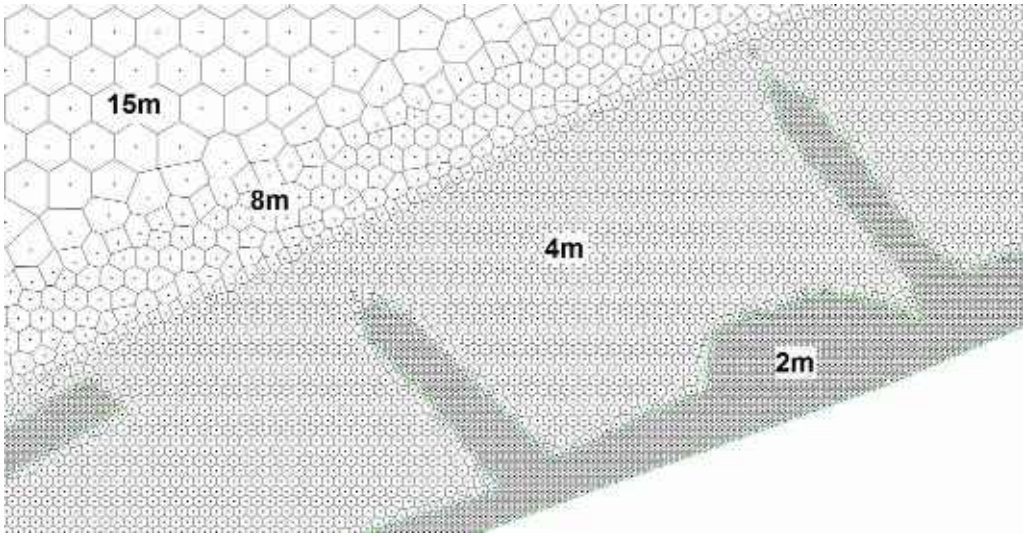


Figure 13 Cell sizes - computational mesh - 3D model Haslau-Regelsbrunn



Figure 14 Computational meh for the 2D model - Vienna-Bratislava

Table 1 and Table 2 are providing information of the used cell sizes for the developed 3D numerical models respectively the 2D numerical model.

Table 1 Overview of used cell sizes for the developed 3D numerical models

	Main channel	Transition zone between main channel and groyne fields	groyne fields	groynes & embankments
	(m)	(m)	(m)	(m)
Haslau-Regelsbrunn	15	8	4	2
Wildungsmauer-Witzelsdorf	15 - 20	8 - 15	4 - 8	2 - 4
Concept model	32	16	8	4

Table 2 Overview of used cell sizes for the developed 2D numerical model

	Main channel	groynes & embankments	side channels	fooldplain
	(m)	(m)	(m)	(m)
Vienna-Bratislava	25	15	5 - 8	30

4.2.1. Boundary conditions

The correct setting of initial and boundary conditions in the model is crucial for the convergence of the numerical model. For steady-state calculation, both the flow at the upper boundary condition, the water level position at the lower boundary condition, and the setting of different surface roughnesses in the model are prerequisites. In addition, the defined boundary conditions impose some assumptions. This necessitates a lead and lag distance to achieve a certain distance from the model reach. As a rule of thumb, a length of the pre- and post-track of about 3 to 5 times the width of the water body is recommended. (BMLFUW / ÖWAV, 2011)

4.2.1.1. Discharge and water level

For the discharges, the known values from the characterizing water levels (KWD 2010) of the Austrian Danube (viadonau, 2012) as well as other significant values were chosen as a basis. Furthermore the water level at the outflow section is presented in the following tables for the modelled reaches.

3D model Haslau-Regelsbrunn:

- RNQ: 980 m³/s 143,54 m.ü.A.
- MQ: 1930 m³/s 144,94 m.ü.A.
- Q3000: 3000 m³/s 145,87 m.ü.A.

3D model Wildungsmauer-Witzelsdorf:

- RNQ: 980 m³/s 139,45 m.ü.A.
- MQ: 1930 m³/s 140,88 m.ü.A.
- Q3000: 3000 m³/s 141,82 m.ü.A.

3D concept model:

- RNQ: 980 m3/s
- Q1800 1800 m3/s
- MQ 1930 m3/s
- Q3000 3000 m3/s

As the schematic model is not based on real terrain data, the water levels were initially based on the characterizing water levels (KWD 2010) of the Austrian Danube (viadonau, 2012), but adapted in the calibration and validation process.

2D model Vienna-Bratislava:

- MQ: 1930 m³/s 137,51 m.ü.A.
- HSQ: 5130 m³/s 140,63 m.ü.A.

4.2.1.2. Roughness values

In 3D models, unlike in 1D or 2D models, Strickler coefficients are usually not used, but equivalent sand roughnesses, whose different roughness values are defined with the help of polygons. The roughness values for bank structures and hydraulic structures at the Haslau-Regelsbrunn model site are derived from experiences of a project site near Haslau on the Danube (Tritthart et al., 2009). Glas et al. (2018) determined roughness values for the modelling reach Wildungsmauer-Witzelsdorf, which were used as a starting point for the calibration and validation procedure. Finally, derived values for equivalent sand roughness are listed below.

3D model Haslau-Regelsbrunn:

- river bed: 0.05 m
- embankments: 0.30 m
- Groyne areas: 0.30 m

3D model Wildungsmauer-Witzelsdorf:

- river bed: 0.03 m
- embankments: 0.30 m
- Groyne areas: 0.30 m

3D concept model:

- river bed: 0.05 m
- embankments: 0.30 m
- Groyne areas: 0.30 m

2D model Vienna-Bratislava

The Strickler coefficients shown in Figure 15 resulted from the calibration and validation of the model. The figure also shows that different roughnesses are included in the model for the floodplain, the main river, and the side channels of the Danube. (Tritthart & Glock, 2018)

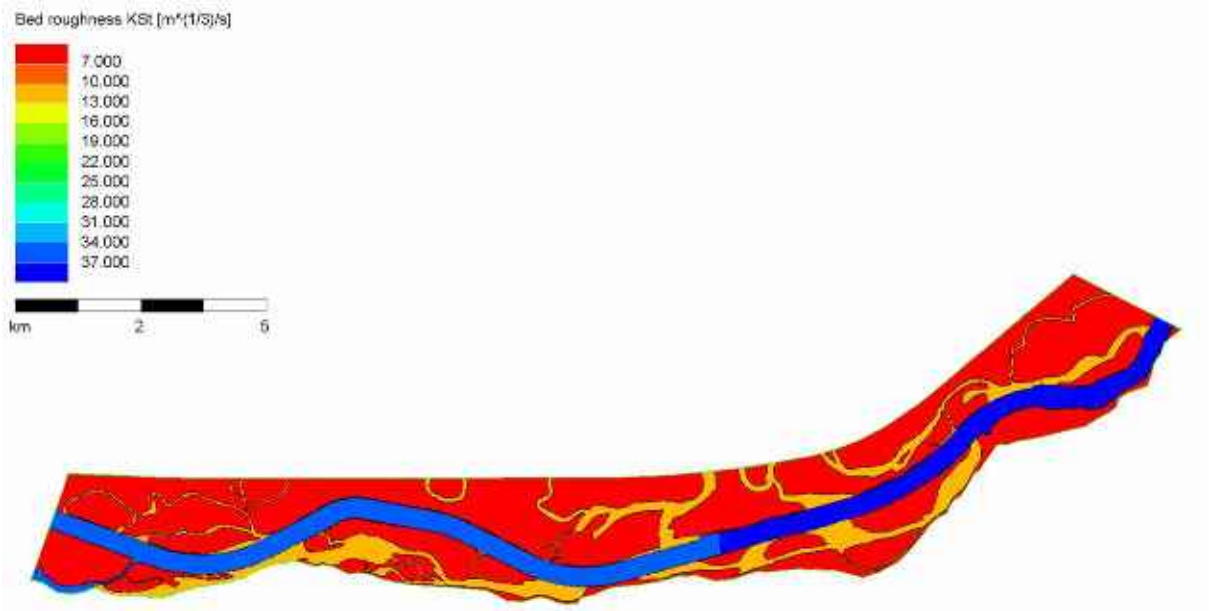


Figure 15 Strickler values for the 2D model Vienna-Bratislava

4.3. Calibration and validation

Those parameters, which are not exactly known as input data in the model, can be determined in such a way that the model represents the real system as accurately as possible. This is done in an iterative process, whereby the insufficiently known model input data is varied within a plausible range of values (Forkel, 2004). Validation refers to the calibrated model that is declared valid. In this process, an independent set of measurement data is used, which

was not used in the calibration. Subsequently, the calculated results are compared with the measured ones, as in the calibration, and the deviations should be within the range of the fitting quality of the model. (BMLFUW/ÖWAV, 2007).

In order to calibrate and validate the numerical models several data sets were used. For some model reaches (i) already calibrated and validated models were available using field data measurements. Another used approach during the calibration and validation process was (ii) using the characteristic water levels (KWD) as well as (iii) newly conducted field data towards water levels, discharge and flow velocities. Field data was gathered mainly in two measurements campaigns between 20.08.2018 and 23.08.2018 as well as between 30.09.2020 and 01.10.2020, whereas the first data set refers to low discharge and the second data set refers to mean discharge conditions. Flow velocities and discharges were conducted using a n ADCP device, water levels were detected with an DGPS device. An overview of the location of the performed measurements is given in Figure 16.



Figure 16 Overview of performed ADCP (red) and water level (orange) measurements at the Danube east of Vienna

The resulting water levels used for calibration and validation are displayed in Figure 17

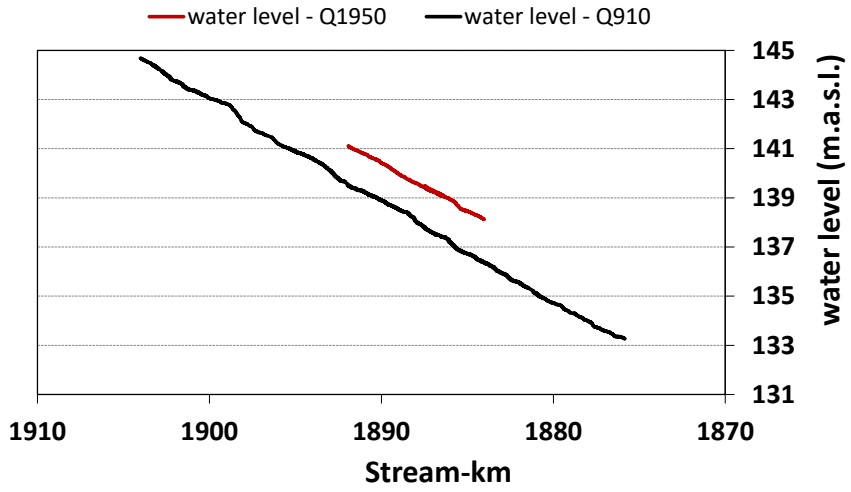


Figure 17 Results of the GPS water level measurement - red: Q1950 m³/s, black: Q 910 m³/s

An example for the detected flow field at stream-km 1886.2 referring to the location of the road bridge in Hainburg for low flow conditions (upper graph) and mean floe conditions (lower graph) is given in Figure 18.

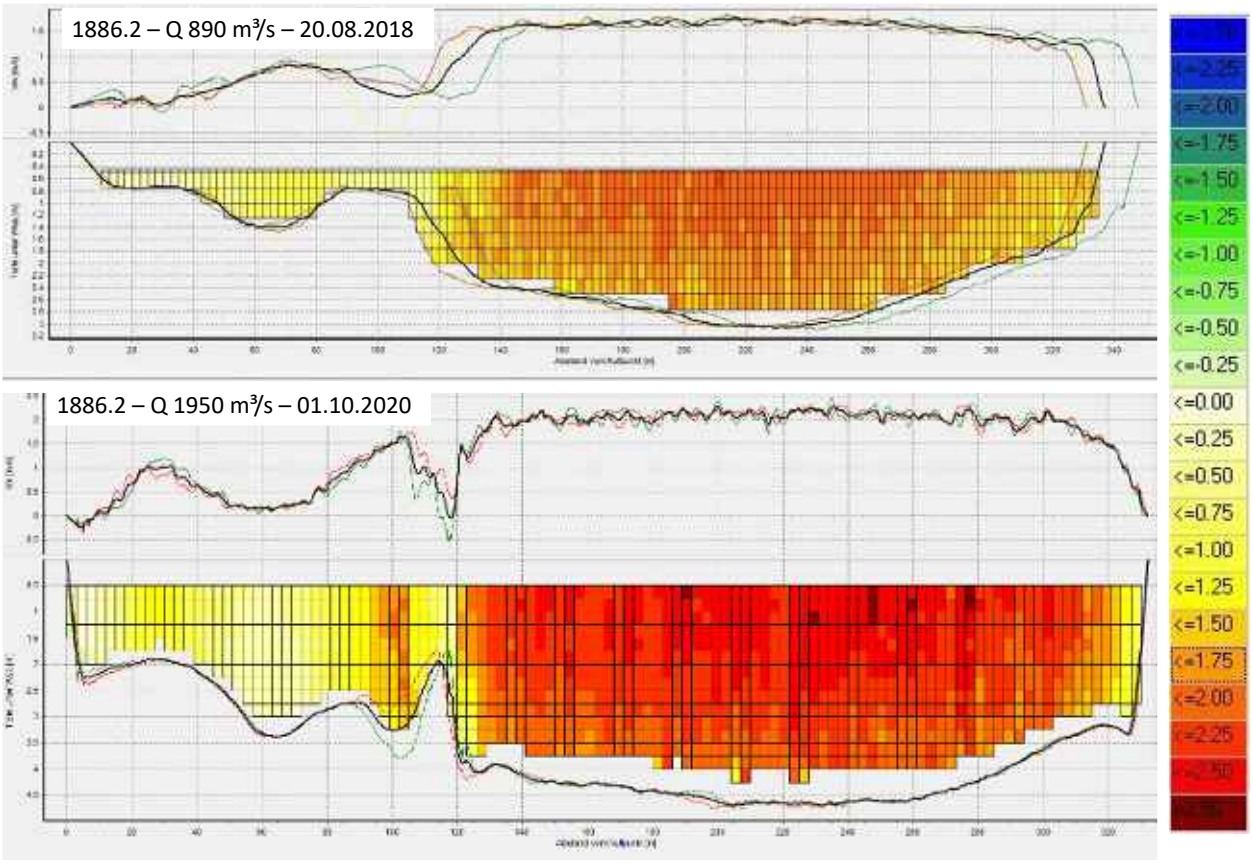


Figure 18 Results of the ADCP flow velocity and discharge measurement – upper graph: Q890 m³/s, lower graph: Q 1950 m³/s

Simulations were performed with given values and the results of the simulation were subsequently compared with the measured values as well as the characteristic water levels. Any deviations were determined and model settings were iteratively improved. It is important that the selected roughness results in a global minimum in the deviation of the water level positions (e.g. minimum of the sum of the error squares).

Compliance with the limits of the basic criteria was checked using the "Residual Monitor" (Tritthart, 2005). Residual values of less than 10^{-3} are considered converged. Figure 19 shows example of the residuals a convergent numerical solution. The criteria used are:

- P pressure
- u, v, w flow velocity in the three spatial directions
- k turbulent kinetic energy
- ε dissipation rate

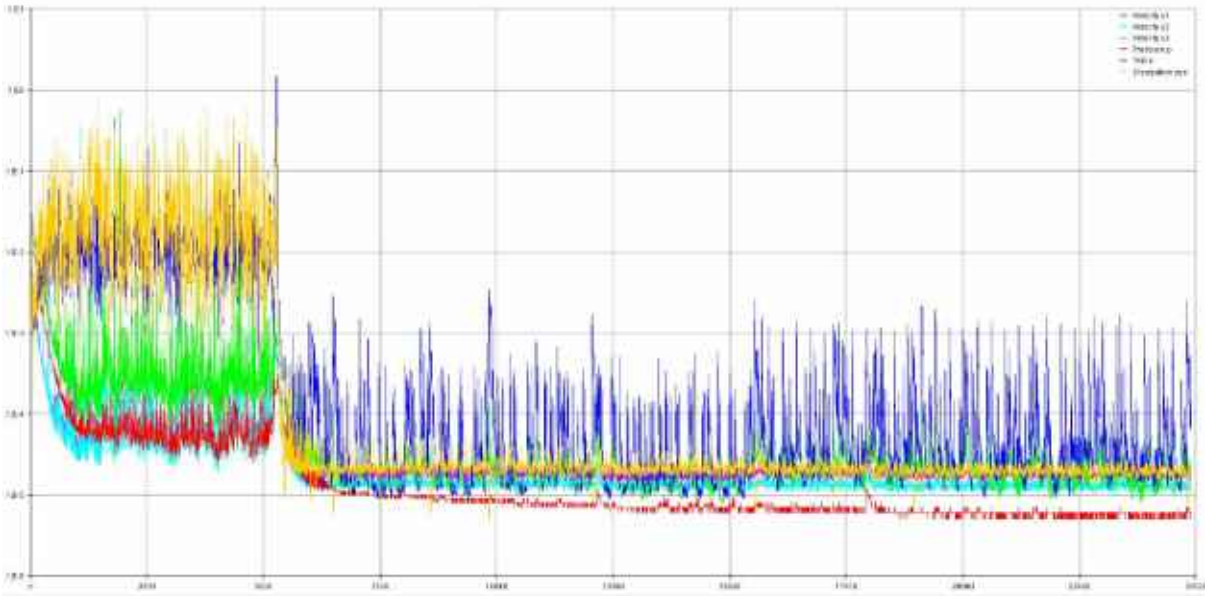


Figure 19 Visualisation of the residuals for a convergent numerical solution

Furthermore the mass gain and losses during the numerical calculation is evaluated. The mass balance should not exceed a deviation of approx. +/- 3%. This is shown for the same modelling result in Figure 20. Only if all criteria are met, the results is considered plausible.

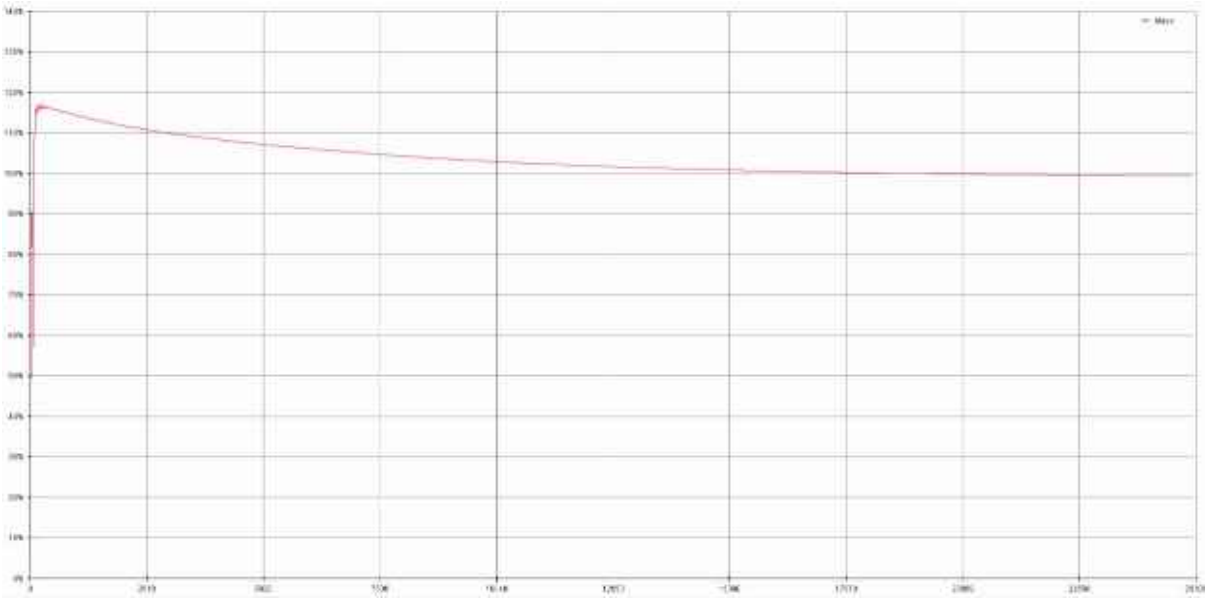
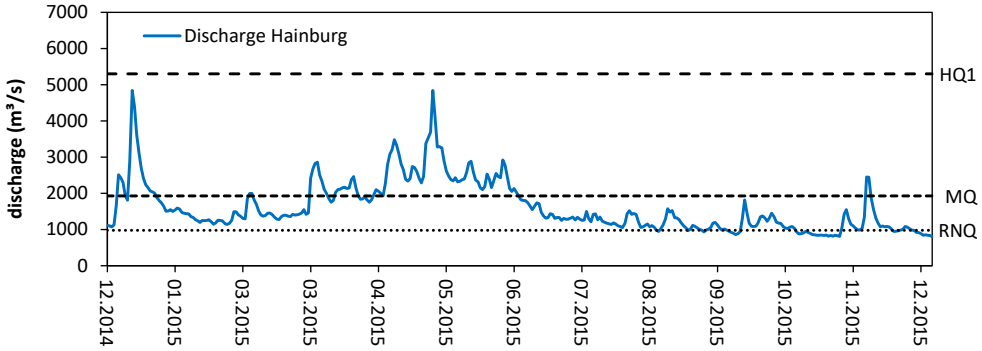


Figure 20 Visualisation of teh mass balance for a convergent numerical solution

4.4. Hydrology

In order to relate the modelling results to a time scale, the hydrology of the Danube River in the project area has been considered. Daily average discharge values from 1977 to 2015 at the gauging station Hainburg were therefore analysed. The hydrograph for the year 2015 is displayed in Figure 21 left, characteristic discharge values are listed in Figure 21 right.



RNQ	980 m³/s
MQ	1930 m³/s
HQ1	5300 m³/s
HQ2	5890 m³/s
HQ5	6620 m³/s
HQ10	7280 m³/s
HQ30	9290 m³/s
HQ100	10400 m³/s

Figure 21 (left) Hydrograph of daily average discharge values, (right) characteristic discharge values - gauging station Hainburg

4.5. Quantification of macro plastic accumulation potential

To derive assumptions of accumulation potential of macro plastic in the project reach, hydrological, numerical and field sampling data is combined. An overview of used field data gathered during bank near samplings BOKU (black), hinterland samplings BOKU (red) and Nationalpark Donau-Auen samplings (green) conducted within the project period is given in Figure 22.

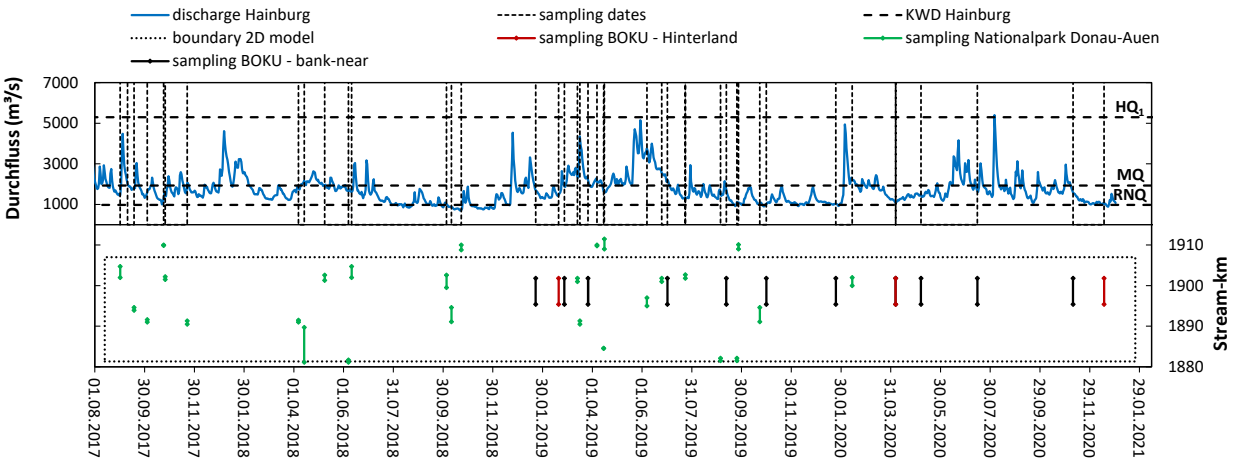


Figure 22 Diagram of hydrograph (blue), bank near samplings BOKU (black), hinterland samplings BOKU (red) and Nationalpark samplings (green) conducted within the project period

Calculations towards the accumulation potential are in particular derived from systematic repetitive samplings as depicted in Figure 23. Sampling points in the Hinterland were defined based on the duration of overflow and therefore the specific discharge. Bank-near sampling points were defined in specific distances to each other and conducted in stripes of 5 m width from the shore line to the beginning of the floodplain.

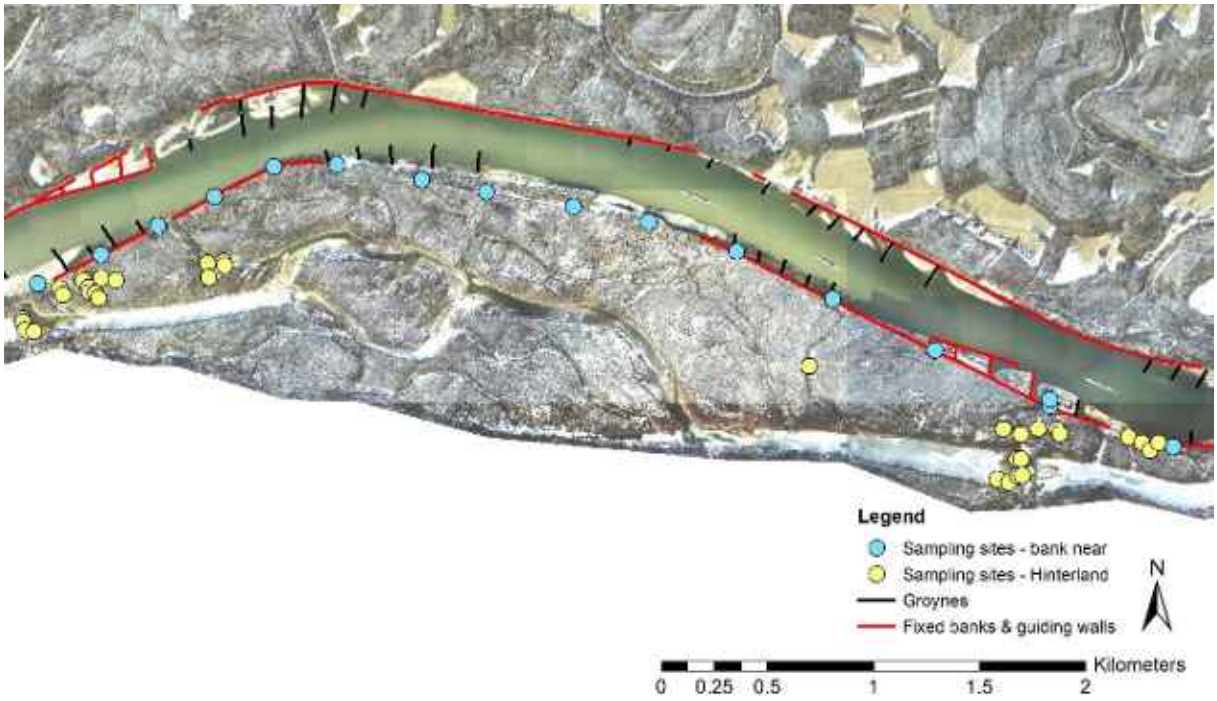


Figure 23 Defined sampling points for repeated bank near and Hinterland sampling of macro plastic

4.5.1. Bank near accumulation zones

A summarized list of the field sampling results conducted in stripes of 5 m width from the shore line to the beginning of the floodplain is presented in the tables below. Table 3 provides data towards observed masses in kilograms, Table 4 contains the number of pieces found in the sampling areas.

Table 3 Bank near macro plastic sampling (BOKU) – mass (kg)

Riverbank Sampling - plastic mass [kg]												
		Sampling	Sample 1	Sample 2	Sample 3	Sample 4	Sample 5	Sample 6	Sample 7	Sample 8	Sample 9	Sample 10	Sample 11
Coordinate X	Coordinate Y	points	22.01.2019	26.02.2019	27.03.2019	02.07.2019	12.09.2019	31.10.2019	24.01.2020	06.04.2020	07.05.2020	15.07.2020	09.11.2020
28684	331557	UP1	0.069	0.026	0.099	0.008	0.089	0.098	0.032	0.111	0.117	0.007	0.397
28982	331694	UP2	0.210	0.197	0.073	0.039	0.010	0.003	0.001	0.024	0.001	0.187	0.011
29250	331831	UP3	0.000	0.014	0.004	0.003	0.001	0.014	0.016	0.008	0.215	0.223	0.050
29517	331969	UP4	0.544	0.000	0.102	0.186	0.096	0.107	0.016	0.058	0.036	0.037	0.173
29799	332109	UP5	0.055	0.000	0.065	0.050	0.001	0.000	0.000	0.000	0.000	0.009	0.034
30096	332119	UP6	0.003	0.015	0.011	0.080	0.002	0.292	0.007	0.000	0.093	0.022	0.001
30496	332048	UP7	0.850	0.078	0.133	0.001	0.054	0.106	0.018	0.041	0.102	0.215	0.271
30800	331990	UP8	1.108	0.114	0.090	no data	no data	1.012	0.186	0.415	0.087	no data	1.427
31212	331921	UP9	0.661	0.763	0.002	no data	0.604	0.010	0.001	0.070	0.000	no data	0.042
31565	331850	UP10	1.055	0.131	0.080	0.098	0.000	0.000	0.003	0.062	0.001	0.032	0.001
31981	331709	UP11	0.674	0.041	0.031	0.017	0.029	1.121	0.154	0.126	0.041	0.026	0.028
32434	331486	UP12	0.027	0.021	0.003	0.026	0.000	0.310	0.001	0.000	0.000	0.002	0.000
32917	331244	UP13	0.012	0.145	0.074	0.043	3.272	0.028	0.053	0.025	0.216	0.262	1.384
33458	330980	UP14	0.602	0.139	0.035	no data	0.653	0.789	no data	0.658	0.318	0.062	0.161
34040	330788	UP15	no data	no data	no data	no data	0.154	0.040	0.021	0.170	no data	no data	3.188
		Sum	**5.870**	**1.684**	**0.799**	**0.551**	**4.964**	**3.930**	**0.507**	**1.768**	**1.226**	**1.084**	**7.168**

Table 4 Bank near macro plastic sampling (BOKU) – number of pieces

Riverbank Sampling - number of plastic pieces												
		Sampling	Sample 1	Sample 2	Sample 3	Sample 4	Sample 5	Sample 6	Sample 7	Sample 8	Sample 9	Sample 10	Sample 11
Coordinate X	Coordinate Y	points	22.01.2019	26.02.2019	27.03.2019	02.07.2019	12.09.2019	31.10.2019	24.01.2020	06.04.2020	07.05.2020	15.07.2020	09.11.2020
28684	331557	UP1	38	36	58	23	43	42	16	45	20	7	36
28982	331694	UP2	109	46	66	78	53	2	1	109	5	63	8
29250	331831	UP3	0	5	14	12	3	5	10	17	7	3	47
29517	331969	UP4	220	0	48	66	16	14	8	81	15	7	42
29799	332109	UP5	51	0	1	9	1	0	0	0	0	2	2
30096	332119	UP6	3	8	1	43	4	8	5	1	19	8	3
30496	332048	UP7	98	15	61	4	33	9	11	9	9	26	10
30800	331990	UP8	229	69	12	no data	no data	278	94	85	31	no data	129
31212	331921	UP9	41	45	3	no data	24	2	1	14	0	no data	3
31565	331850	UP10	5	42	36	11	0	0	1	10	4	19	2
31981	331709	UP11	3	25	15	23	45	13	14	37	11	9	5
32434	331486	UP12	5	3	3	6	0	13	1	0	1	3	0
32917	331244	UP13	29	51	49	60	51	64	18	37	20	31	22
33458	330980	UP14	64	40	1	no data	48	2	no data	38	10	31	43
34040	330788	UP15	no data	no data	no data	no data	89	1	3	30	no data	no data	70
		Sum	895	385	368	335	410	453	183	513	152	209	422

In the following the procedure to combine numerical model results with sampling data and hydrological data is described

- Hydrological analysis of period between 2 samplings
  - Determination of descending water level duration
  - Determination of modelled discharges for mass calculation
- Determination of areas for calculation of accumulation potential
  - Maximum water level minus sampling water level in the bank near region
  - Determination of influence length between neighbouring sampling point
  - Determination of length between the shore lines (min/max water level) at each sampling points
  - Calculation of separate areas for the influence width of each sampling point
- Calculation of concentrations and total accumulation was performed in different ways
  - Using average concentration over all sampling points multiplied with estimated sub-area based on sampled length between sampling and maximum water level at each sampling point
  - Determination of sub-area concentration for each sampling point multiplied with estimated sub-area based on sampled length between minimum and maximum water level at each sampling point
  - Determination of sub-area concentration for each sampling point multiplied with estimated sub-area based on sampled length between minimum and maximum water level at each sampling point
  - Determination of sub-area concentration for each sampling point multiplied with sub-area exported from 2D numerical model

In Figure 24 a sketch towards the methodology for combination of sampling data with hydrological and numerical data to describe bank near accumulation potential is depicted.

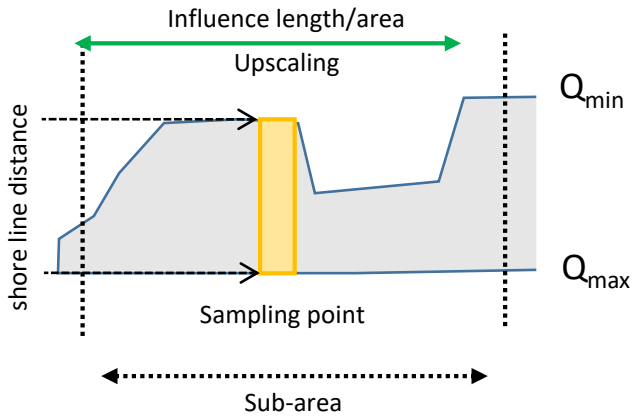


Figure 24 Sketch of the methodology towards combination of sampling data with hydrological and numerical data to describe bank near accumulation potential

4.5.1. Floodplain accumulation zones

As shown in Figure 23 repeated samplings of macro plastic also were performed in the floodplain area. Sampling was conducted in various predefined areas covering inflow and outflow sections in the side channel system, accumulation areas related to woody debris as well as such areas only submerged rarely by extreme events. In order to analyse the sampled plastics on a hydrological and hydraulic basis various analysis were performed:

- Quantification of discharge in the side channel systems related to the Danube discharge
- Flow velocity and water depth in the sampling areas were determined from numerical models
- Specific discharge was calculated
- Analysis towards elevation and vegetation was performed

5. Results

The evaluation and discussion of the results takes place in a concrete differentiation of the models.

5.1. 3D numerical models

The visualization of the simulations in the postprocessor is done for the RNQ, Q1800 (concept model), MQ and Q3000 discharges. Numerical model results in general offer broad possibilities for visualisation. In the following chapters the most important parameters are presented in order to derive findings towards macro plastic transport in the modelled reaches:

- Flow velocity
- bed shear stress
- water levels

Within the 3D numerical models, the flow velocities were calculated distributed over the water depth for 6 layers. The representation of the flow velocities is done for surface layer.

5.1.1. 3D model Haslau-Regelsbrunn

5.1.1.1. Flow velocity

For regulated low flow (RNQ) the maximum flow velocities at the near-surface layer are about 2.4 m/s (see Figure 25 top). These occur at about the level of the right bank guiding structure, as well as at the left bank groynes downstream of the model area. As a result of the curvature in the river course, secondary flows are also induced that overlap with the main flow. The result is the formation of a vortex flow, which shifts the maximum of the main flow towards the outer bank. (Giesecke, 2014) A significant reduction in flow velocities occurs on the right bank in the groyne fields, where flow velocities barely exceed 0.3 m/s. The highest velocities in the groyne fields show up in the transition area from the groyne field to the main stream with up to 1.2 m/s. Since there is little interaction between the main stream and the groyne field during low flow, the majority of the water in these flow-calmed zones eventually comes to a standstill.

Compared to the regulated low flow (RNQ) of the regulating system, significantly higher flow velocities of up to 2.7 m/s occur in the main stream at mean discharge MQ (see Figure 25 centre). Looking at the area behind the guiding structure, it can be seen that due to the partial overflow, the flow velocities locally increase to up to 1.5 m/s. Although overflow is already taking place at the groyne heads, the flow velocities in the right bank groyne fields remain low.

At a discharge of 3000 m^3/s, clear increases in velocity can be seen compared to mean and low water, as Figure 25 bottom illustrates. Especially downstream of the last right bank groyne, flow velocities of up to 3 m/s occur. Likewise, near the tailrace, maximum flow velocities occur due to the constriction of the cross-section, as well as due to occurring secondary currents. Behind the guiding structure, flow velocities of up to 2.1 m/s can be observed, while lower velocities of up to 1.8 m/s are calculated within the groyne fields.

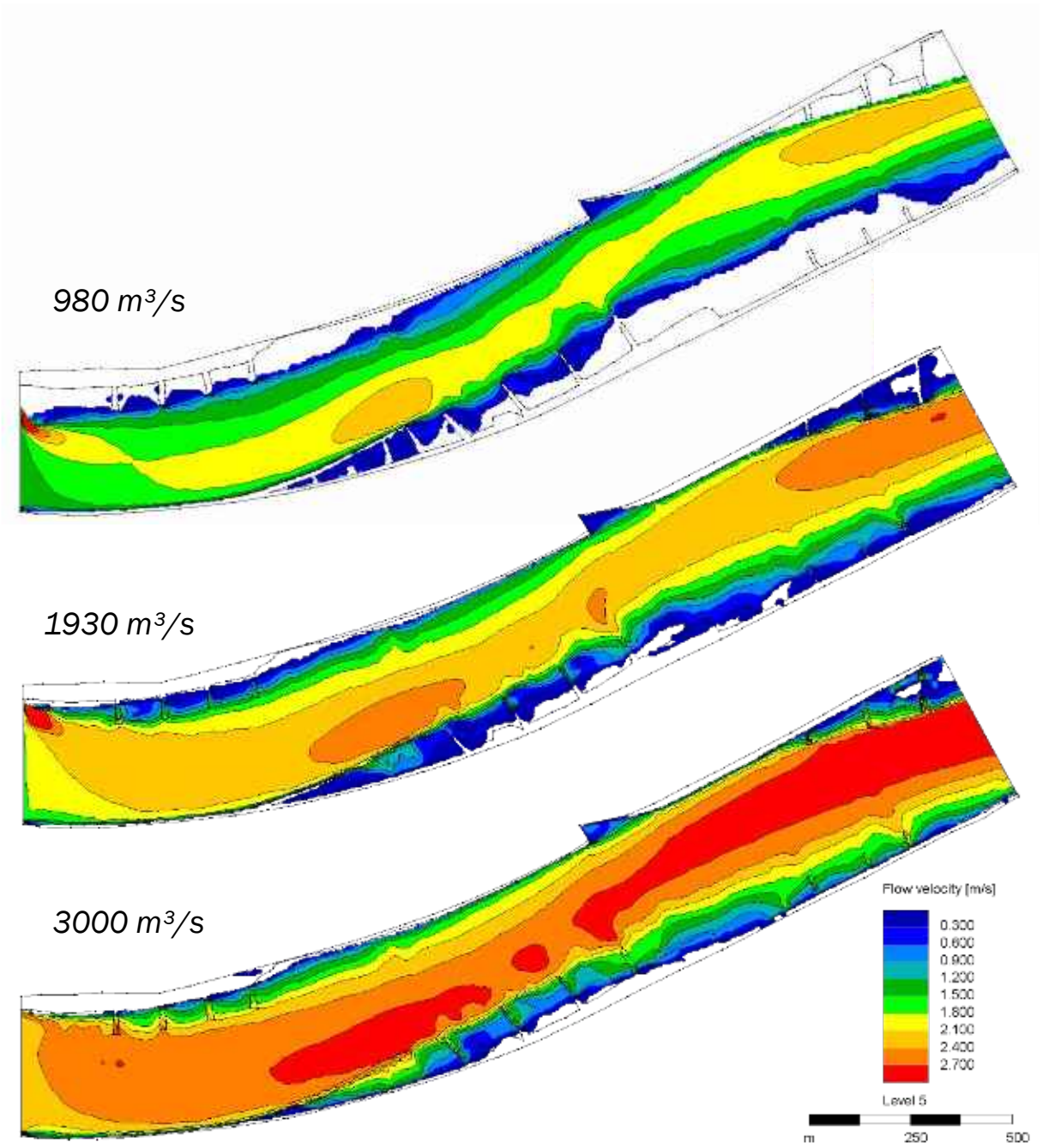


Figure 25 3D model Haslau-Regelsbrunn - flow velocity – top: RNQ 980 m³/s, centre: MQ 1930 m³/s, bottom: Q 3000 m³/s - surface near layer

5.1.1.2. Bed shear stress

During regulated low flow (RNQ) (Figure 26 top) the values for bed shear stress are low corresponding to the low flow velocities at this discharge. The areas of maximum bed shear stresses coincide with those areas where maximum flow velocities occur, as a result of the secondary flows. Particularly on the right bank in the model area, hardly any noteworthy bottom shear stresses can be observed.

According to the higher discharge, there are more areas where maximum bed shear stresses of up to 20 N/m² occur during mean discharge conditions MQ (Figure 26 centre). Although a general increase of the bed shear stresses in the main channel is evident, values in the groyne fields still hardly reach more than 2 N/m².

At a discharge of 3000 m³/s, bottom shear stresses of 20 N/m² or higher occur almost everywhere in the main channel (Figure 26 bottom). However, a significant increase in bed shear stress is also present downstream of the guiding wall and in the downstream groyne field.

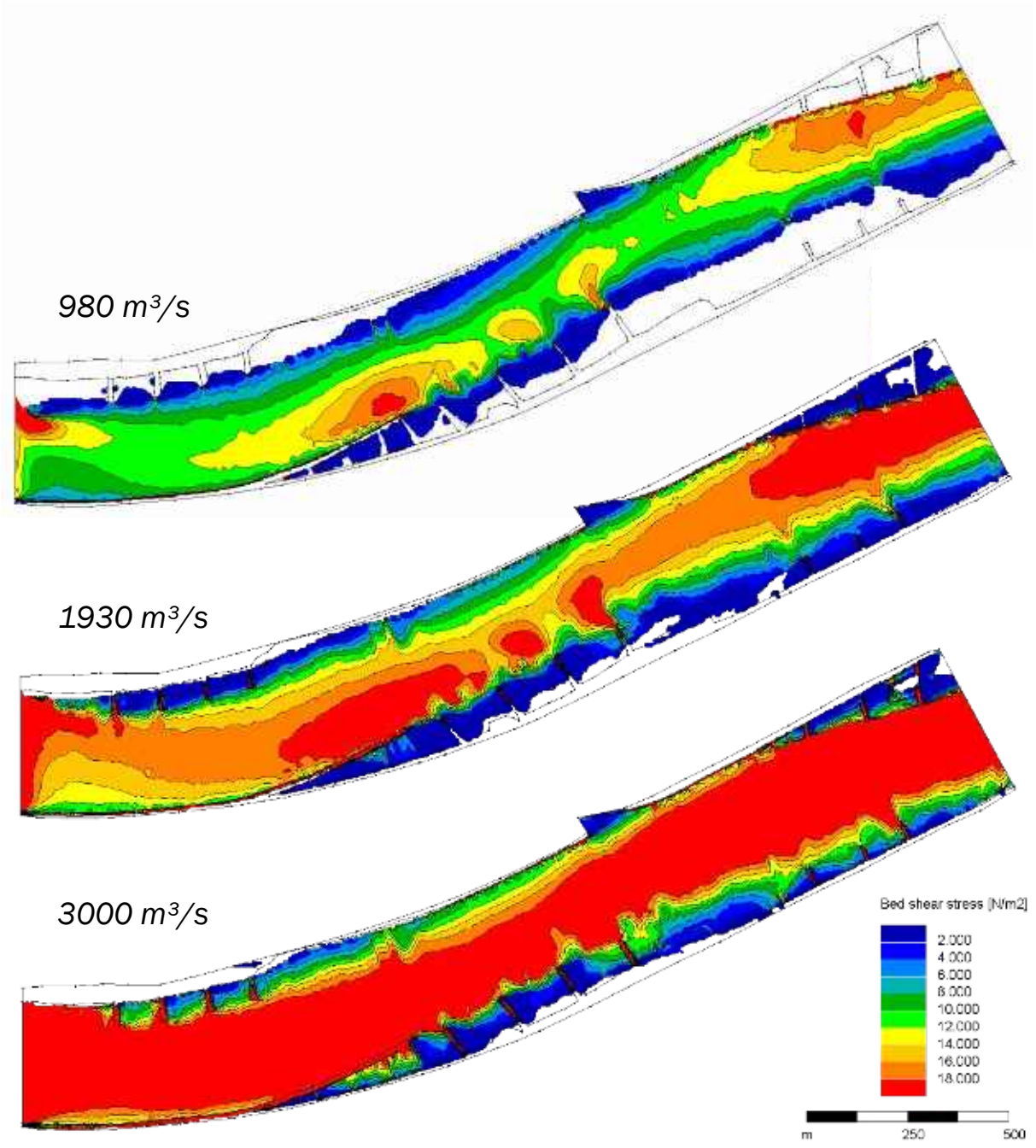


Figure 26 3D model Haslau-Regelsbrunn – bed shear stress – top: RNQ 980 m³/s, centre: MQ 1930 m³/s, bottom: Q 3000 m³/s - surface near layer

5.1.1.3. Water level

The representation of the water level primarily gives an impression of the gradient of the water level, which is characterized by the distance of the boundary lines between two colour areas. While a steep water level gradient is first recorded during regulated low flow (RNQ) (Figure 27 top), this is followed by uniformly shallow gradients, with

the gradient increasing again towards the end of the model reach. The elevated water level behind the tailrace is probably due to the water level pre-estimation, which was set higher in this area. Thus, the area there is no longer connected and the original water surface elevation remains approximately the same.

No considerable changes in the characteristics of the water level can be seen at mean discharge compared to regulated low flow (RNQ) (Figure 27 centre). However, the main difference is the area downstream of the guiding structure, where a similar water level position as in the main stream is observed. This is due to the fact that the area is connected to the main stream at this flow.

On the basis of Figure 27 bottom, at a discharge of 3000 m^3/s, it can be seen above all that the guiding structure and the groynes are completely submerged. Water level gradients appear to be uniform.

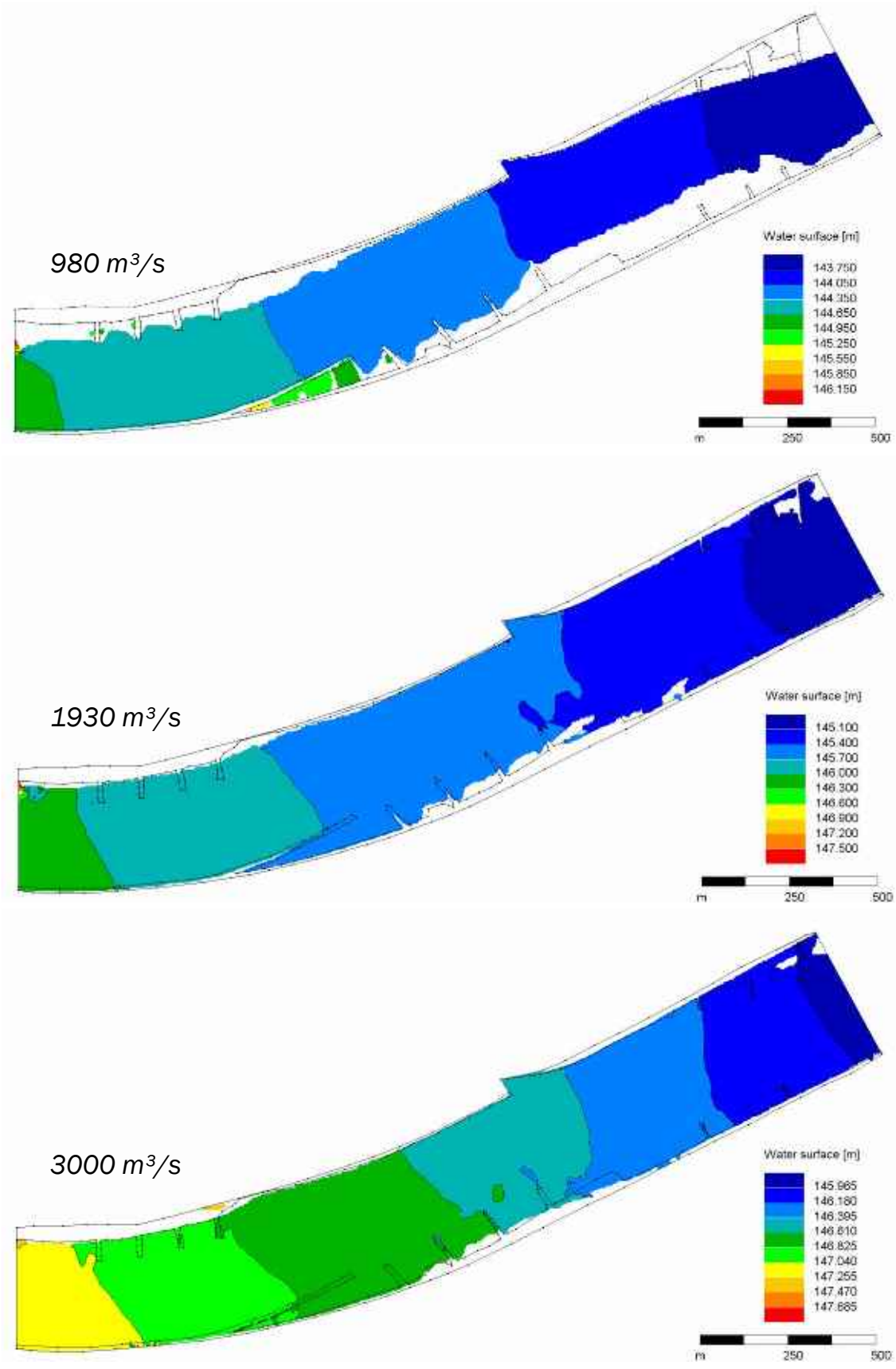


Figure 27 3D model Haslau-Regelsbrunn – water level – top: RNQ 980 m³/s, centre: MQ 1930 m³/s, bottom: Q 3000 m³/s

5.1.2. 3D model Wildungsmauer-Witzelsdorf

5.1.2.1. Flow velocity

During regulated low flow (RNQ) conditions the highest flow velocities occur with up to 2.4 m/s in the model downstream of the left bank guiding unit near the first groyne head (Figure 28 top). Upstream on the right bank from the guiding structure, flow velocities reach their maximum at about 1.5 m/s in the main channel. The largest stillwater zones in terms of area occur downstream of the left bank guiding wall and on the right bank groyne fields near the downstream end of the model reach.

A clear increase in velocity can be observed at mean discharge conditions (MQ) compared to regulated low flow (RNQ) situation (Figure 28 centre). In the upstream part of the model until the left bank guiding wall a large zone of flow velocities of more than 1.8 m/s can be observed. In the following section the flow velocities increase to ca. 2.4 m/s in the main channel as a result of the narrowing effect induced by the left bank guiding wall and the groyne field as well as the right bank groyne field in the downstream section. Within the groyne field still zones of more or less no flow velocities can be observed, as the groynes are only slightly submerged at this water level.

For a discharge of 3000 m^3/s maximum flow velocities of up to 3 m/s can be seen near the stillwater zone of the right bank groyne field in the downstream end of the model and locally at the guiding wall (Figure 28 bottom). A clear increase in velocity compared to midwater is also evident in the upstream area, where flow velocities of up to 2.4 m/s occur. In addition, a greater interaction between main channel and the groyne fields can be observed. However, in the downstream right bank groyne field zones with very low flow velocities still are evident.

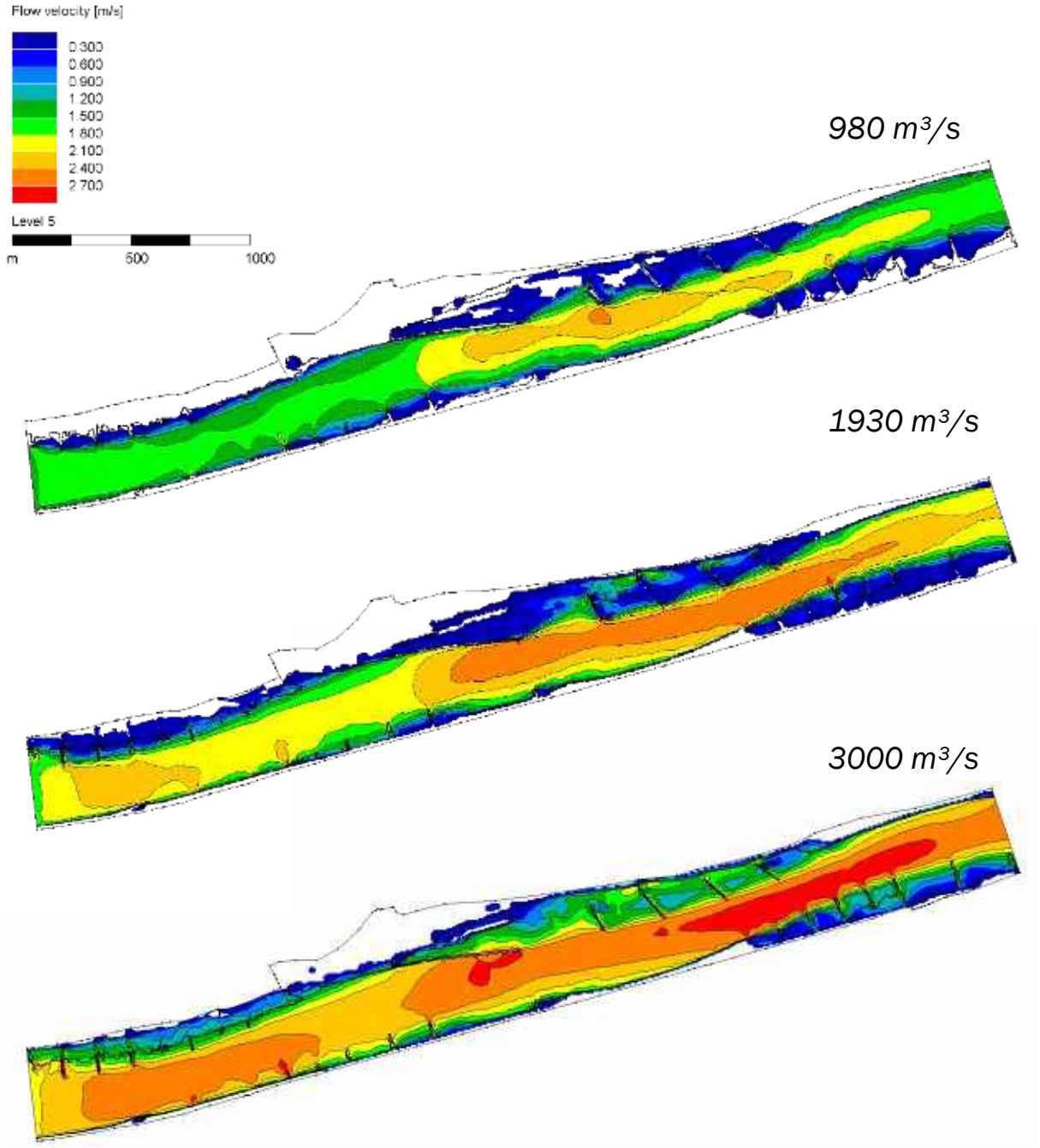


Figure 28 3D model Wildungsmauer-Witzelsdorf - flow velocity – top: RNQ 980 m³/s, centre: MQ 1930 m³/s, bottom: Q 3000 m³/s - surface near layer

5.1.2.1. Water level

Looking at the water levels at regulated low flow (RNQ) condition (Figure 29 top), it can be seen that a uniformly flat gradient occurs up to the left bank guiding structure, which then becomes steeper due to constrictions induced by the guiding wall. Toward the end of the model, the slope reduces again. In addition, the impounding effect of individual groynes can be seen. More or less the same picture is drawn during mean discharge conditions MQ (Figure 29 centre), except that the left bank groynes downstream of the guiding wall are already submerged at this discharge. For a discharge of 3000 m³/s a total overflow of the hydraulic structures in the entire model area can be observed, leading to a very homogeneous water level gradient in general (Figure 29 bottom).

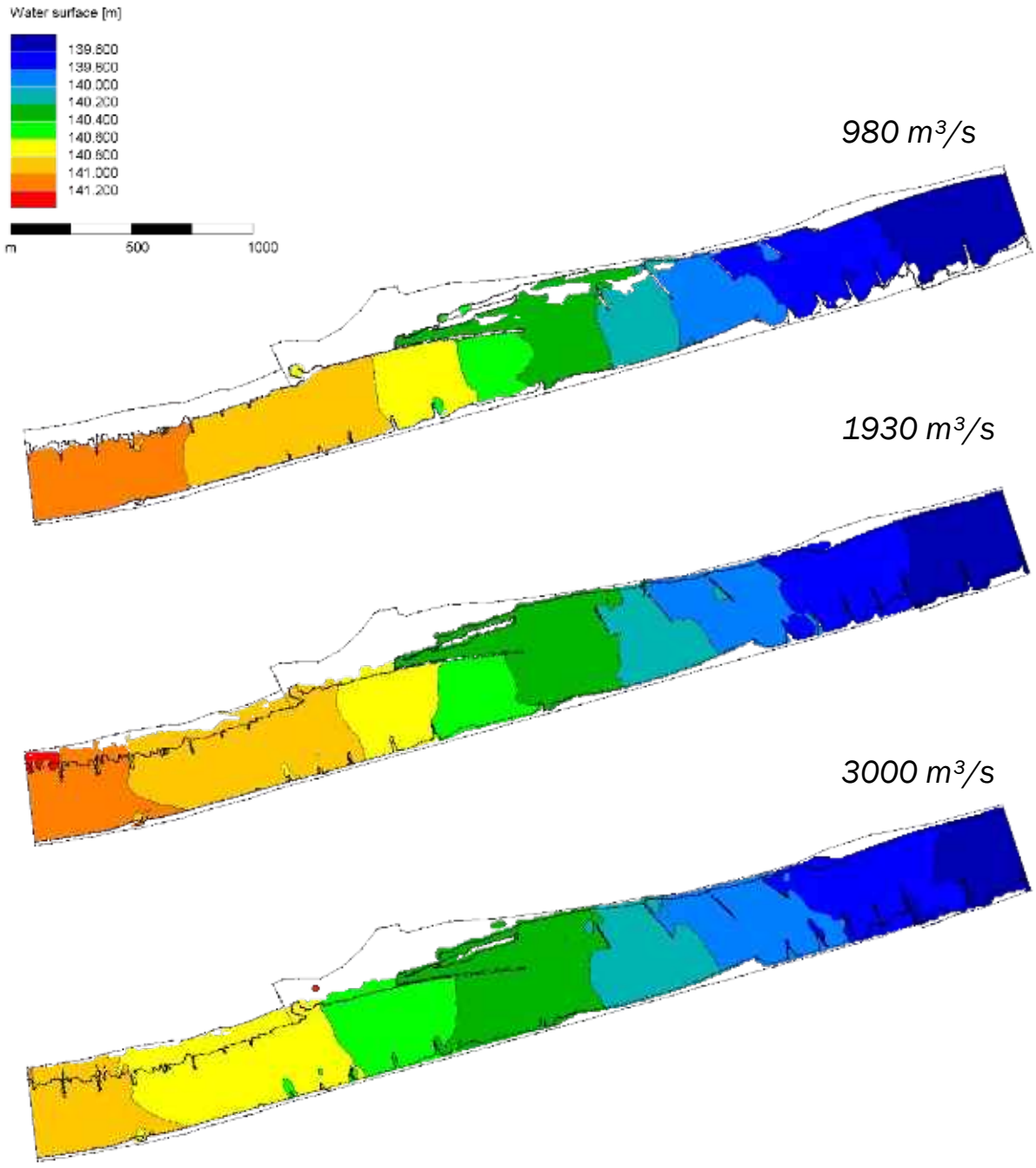


Figure 29 3D model Wildungsmauer-Witzelsdorf – water level – top: RNQ 980 m³/s, centre: MQ 1930 m³/s, bottom: Q 3000 m³/s

5.1.3. 3D concept model

In the following chapters exemplarily representative results of the 3D numerical modelling are presented.

5.1.3.1. Flow velocitiy

In the simplified plane bed model (Figure 30 top) depth average flow velocities appear to be very constant in the centre of the river around 1.40 m/s. Still water zones with low velocities are visible in the groyne fields for this discharge level, since there is only a minor interaction between the main channel and the groyne fields. A similar picture with minor changes can be seen in model 2 (Figure 30 centre), referring to the geometry including inner and

outer bend characteristics. Due to the flow constriction of the downstream left bank groyne field and the inner bank, flow velocities of up to 2.2 m/s occur.

The difference plot between the two models it can be easily seen, that flow velocities for model 2 are higher on the outer bend sections (red), while on the inner bank there is a velocity reduction (blue), due to the fact that the different geometry directs the flow towards the outer bend.

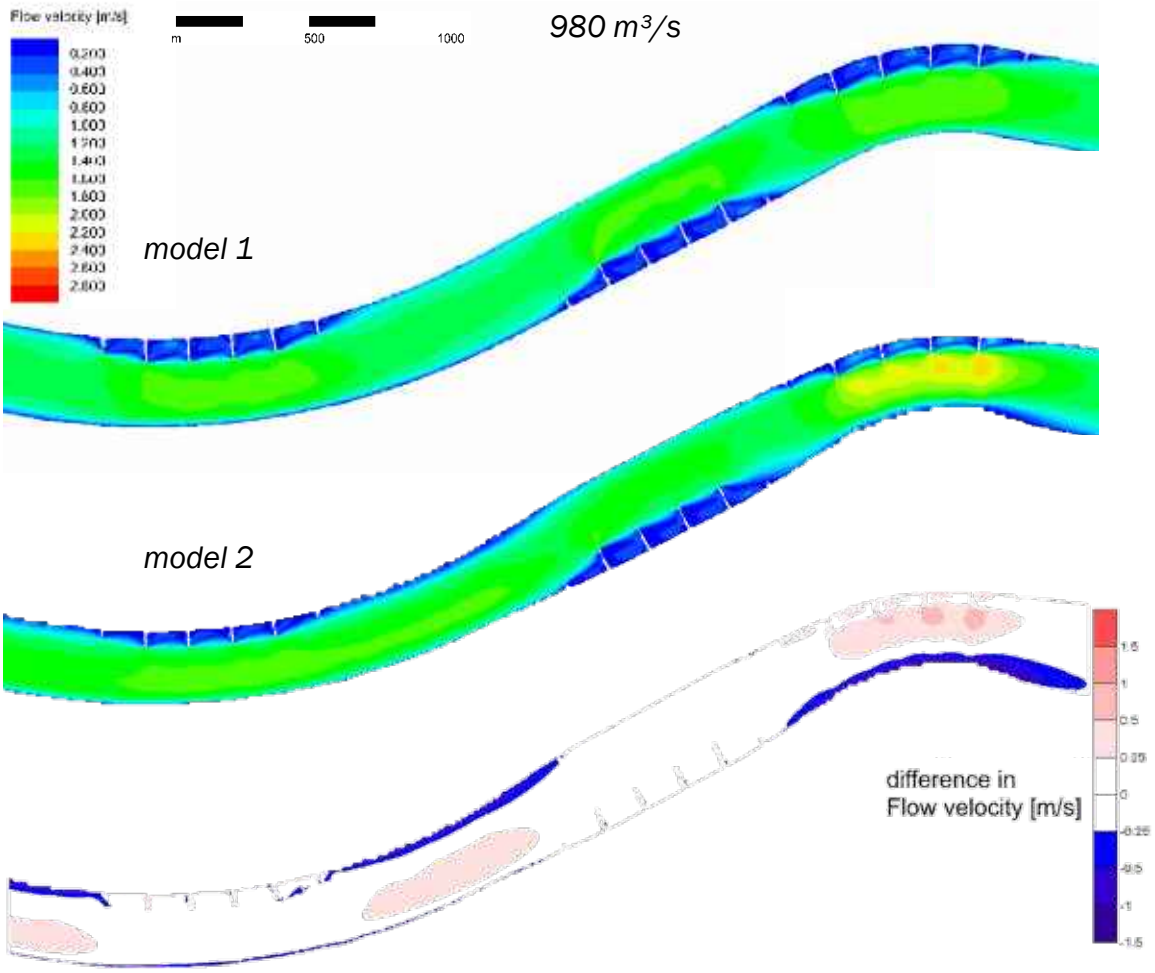


Figure 30 3D concept model – flow velocity – RNQ 980 m³/s – top: model 1, centre: model 2, bottom: difference plot (model 2 minus model 1)

Compared to regulated low flow (RNQ), a considerable increase in velocities is recognized at a discharge of 3000 m³/s (see Figure 31). The maximum velocities range between 2.6 to 2.8 m/s. In both model 1 and model 2, all groynes are submerged. Still, large areas of low flow velocities are found within the groyne fields. Maximum flow velocities result in the main channel at the location of the groyne fields, due to constrictions of the cross section. As for regulated low flow (RNQ), model 2 leads to higher maximum flow velocities compared to model 1 with a flow concentrated more towards the outer banks. Further differences are visible in the upstream left bank groyne field with more overflow and therefore higher flow velocities occurring in model 2 with the more natural geometry.

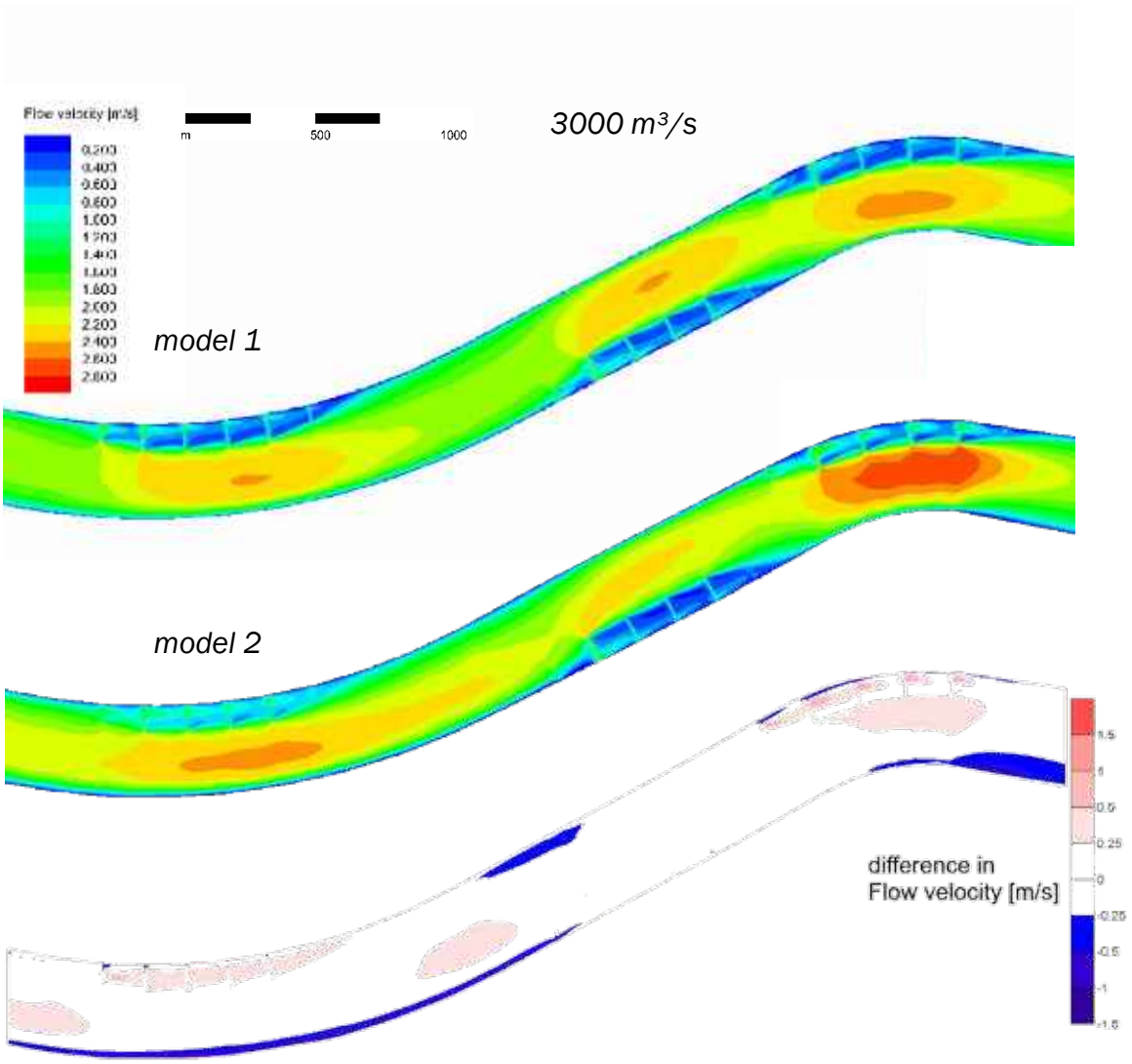


Figure 31 3D concept model – flow velocity – Q 3000 m³/s – top: model 1, centre: model 2, bottom: difference plot (model 2 minus model 1)

In Figure 32 exemplarily the comparison of the depth average flow velocity between model 2 and model 3 is presented for the medium flow conditions (MQ) of 1930 m³/s. All groynes are slightly submerged at this discharge level. In the main channel, a similar constant velocity of about 1.60 – 1.80 m/s can be observed in both model variants upstream and downstream of the engineering structures. The maximum flow velocity is approx. 2.30 m/s for both models, differences here are clearly visible. While in model 2 the area of increased flow velocities due to the cross sectional constriction is distributed over the whole length of the groyne field, in model 3 the maximum flow velocities are more concentrated at the single groyne reaching a higher increase of values therefore. Between the single groynes of the groyne field in model 2, flow calmed zones are found due to the low interaction with the main channel. In Model 3 only one large still water zone, related to a vortex formation downstream of the single groyne evolves.

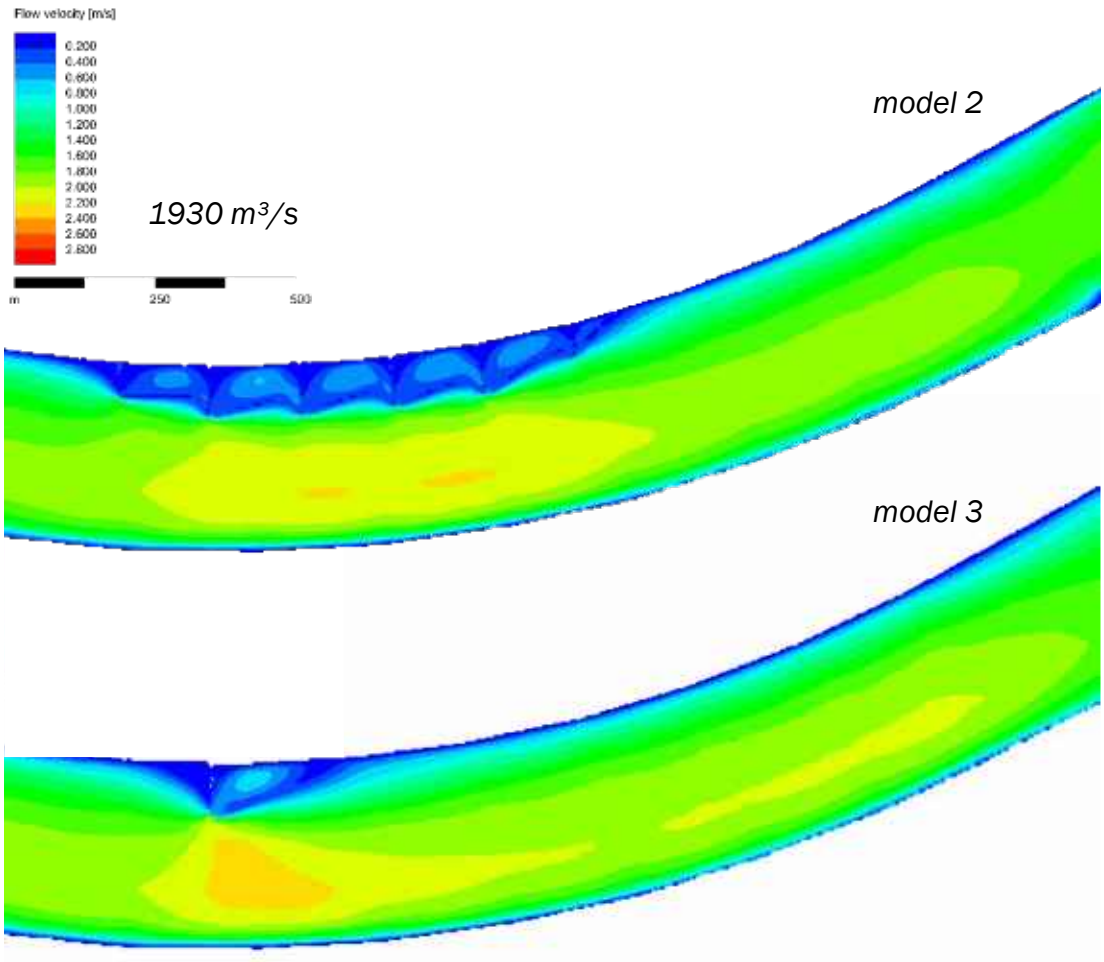


Figure 32 3D concept model – flow velocity – MQ 1930 m³/s – top: model 2, bottom: model 3

5.1.3.2. Water level

The distance of the boundary lines between two colours areas give an impression of the gradients of the water level. The closer they are together, the steeper the gradient. During low water level in the highly simplified model 1 (Figure 33 top), the gradient is very even while model 2 (Figure 33 bottom) shows a somewhat flatter gradient at the beginning and becomes somewhat steeper in the area of the downstream right bank groyne field related to the general differences in geometry with inner and outer bank profiles.

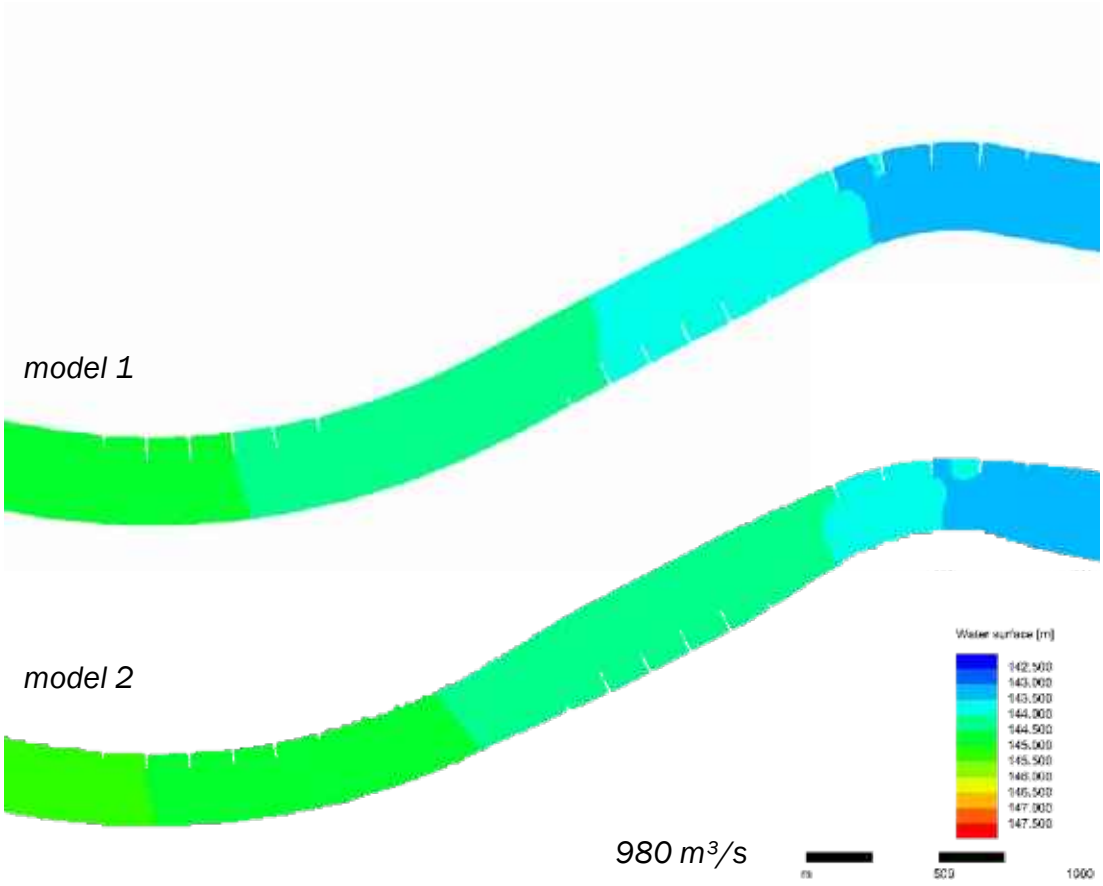


Figure 33 3D concept model – water level – RNQ 980 m³/s – top: model 1, bottom: model 2

Results of the calculated water levels for model 1 and model 2 at a discharge of 3000 m³/s are depicted in Figure 34. Basically, a rather homogeneous water level gradient prevails in both models, however, in the second model a higher gradient is recognizable due to the more constrained cross sections.

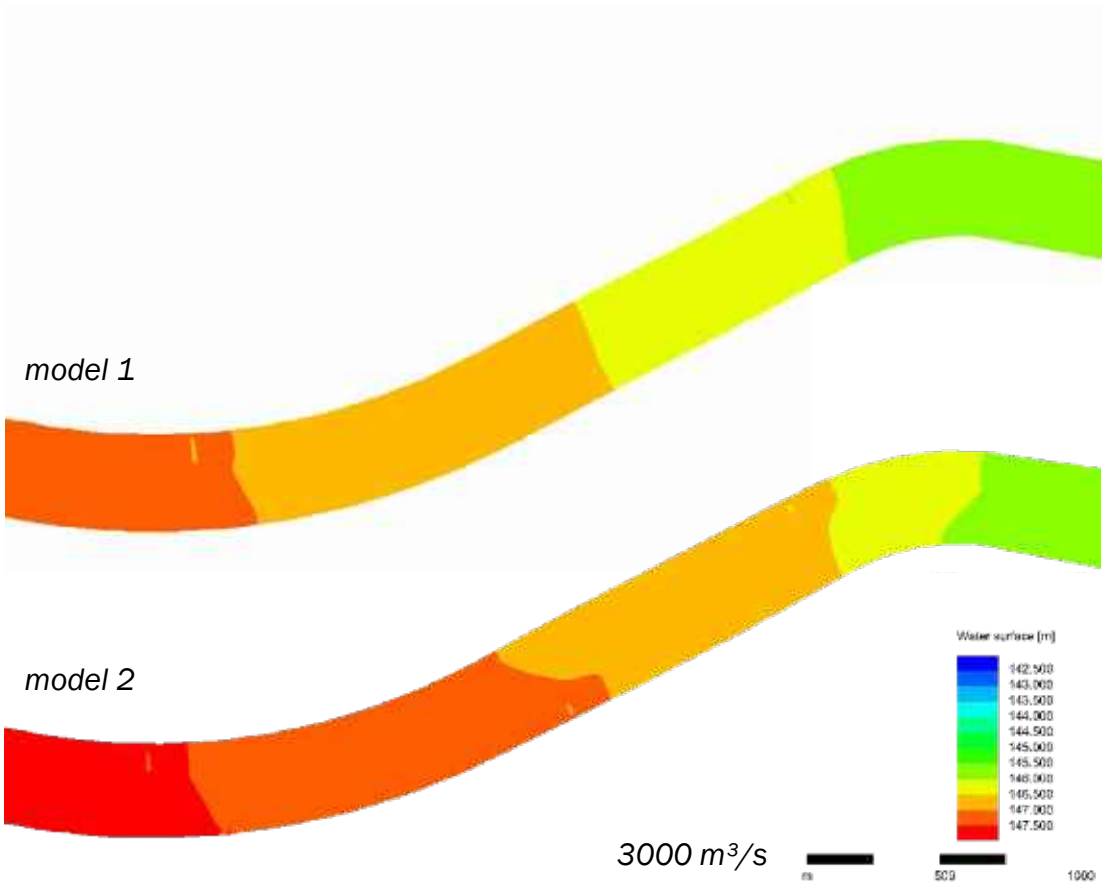


Figure 34 3D concept model – water level – Q 3000 m³/s – top: model 1, bottom: model 2

5.2. 2D numerical model

For the 2D numerical model created, solution files were calculated in increments of 400 m³/s between 400 m³/s and 10800 m³/s, according to the characteristic water levels additional discharges were calculated. The focus of the 2D model is mainly towards the accumulations in the bank near areas as well as in side branches and inundation areas. This was performed using water level data from the model, hydrological data as well as sampling data provided by ABF/BOKU conducted within the scope of the project. The following parameters are presented as results of hydrodynamic modelling:

- Flow velocity
- water depth
- Water levels
- Bank near accumulation
- Floodplain accumulation

5.2.1. Flow velocity

In Figure 35 the depth average flow velocities for the 2D numerical model Vienna-Bratislava is depicted. The sequence charts shows a subsequent increase of flow velocity in the main channel with increasing discharge, especially for the flood discharge of 5.130 m³/s and the flood event with a reoccurrence interval of 100 years referring to a discharge of 10.400 m³/s at the bottom of the figure. During this discharge event also all of the

inundation area is submerged. Only slow velocities occur in the floodplain, however, the secondary side channel are visible due to the flow velocities.

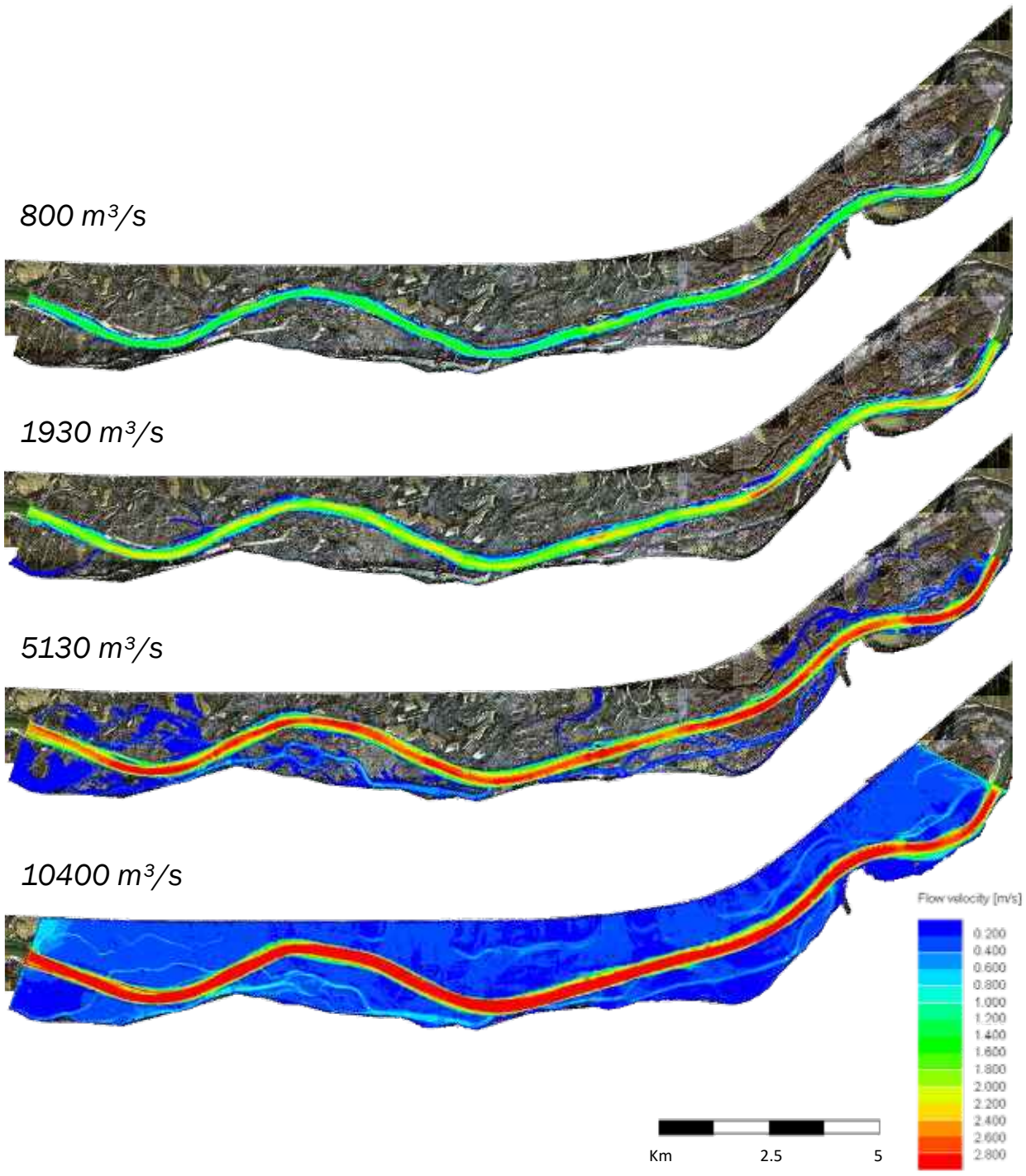


Figure 35 2D model Vienna-Bratislava – flow velocity – RNQ 980 m³/s, MQ 1930 m³/s, HSQ 5130 m³/s, HQ_{100} 10400 m³/s

5.2.2. Water depth

In Figure 36 the water depth of the 2D numerical model Vienna-Bratislava are depicted in the same way. As for the flow velocities, a subsequent increase of the water depth with increasing discharge is visible. Beginning at the

discharge of 5.130 m³/s the secondary side channels and parts of the inundation are submerged. For the flood event with a reoccurrence interval of 100 years referring to a discharge of 10.400 m³/s the water depth in the whole main channel exceeds 7 meters, even in wide parts of the inundation area water depth of 2 to 4 meters can be observed.

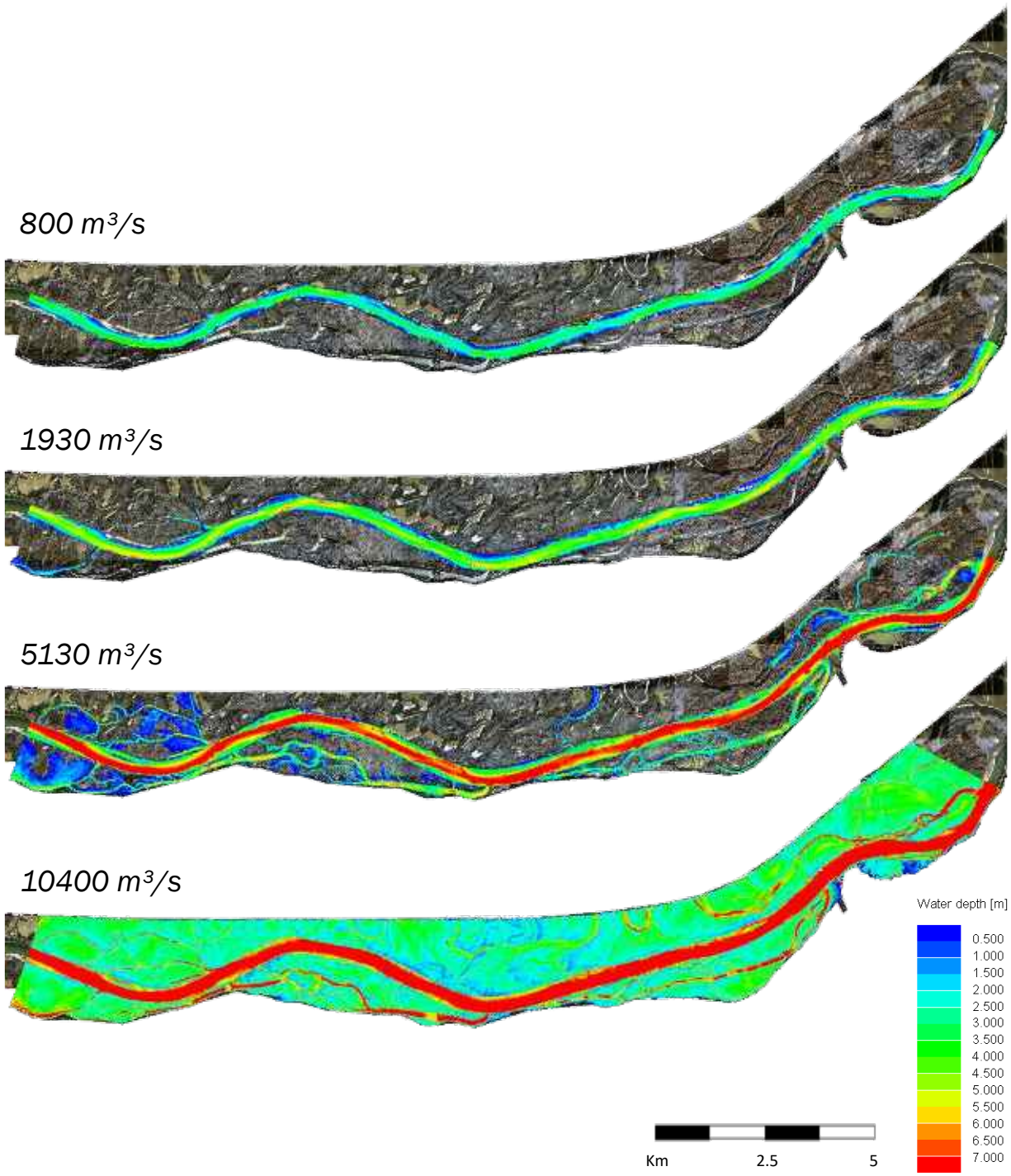


Figure 36 2D model Vienna-Bratislava – water depth – RNQ 980 m³/s, MQ 1930 m³/s, HSQ 5130 m³/s, HQ100 10400 m³/s

5.2.3. Water levels

Together with bank near and floodplain macro plastic samplings the derived water levels build the basis towards a large scale analysis of macro plastic accumulation. Examples for the exported water level data from the 2D numerical model Vienna-Bratislava are presented in Figure 37 for the discharges of 800 m³/s, 1930 m³/s, 5130 m³/s and 10400 m³/s. A detailed map of the result showing the overflow of the inundation area with rising discharge near Haslau is provided in Figure 38.

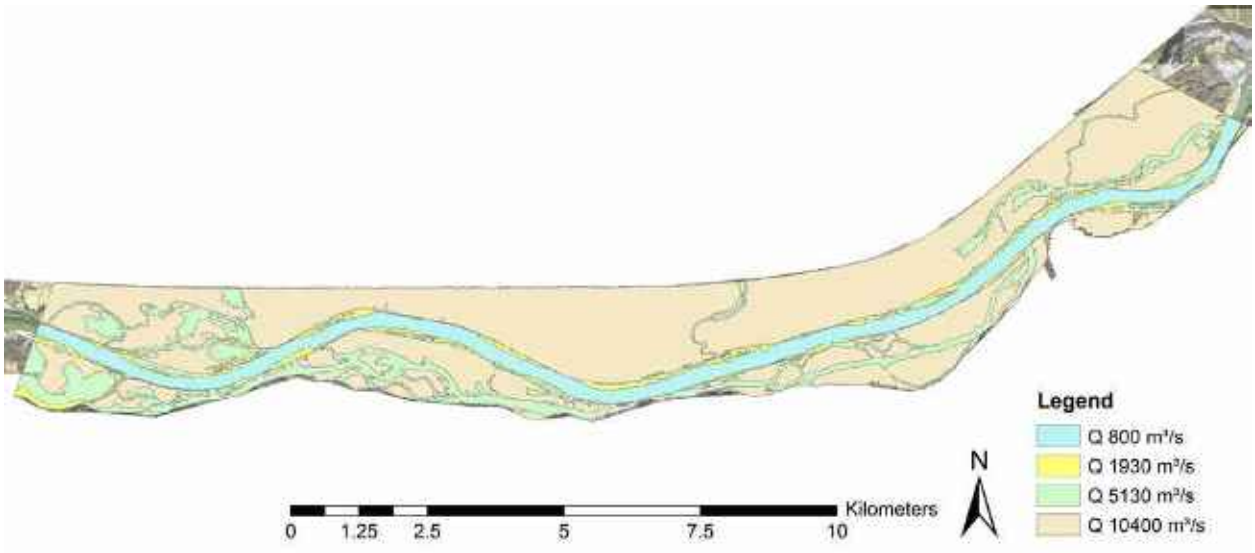


Figure 37 Map of water levels – 2D model Vienna-Bratislava – examples – blue: 800 m³/s, yellow: 1930 m³/s, green: 5130 m³/s, orange: 10400 m³/s

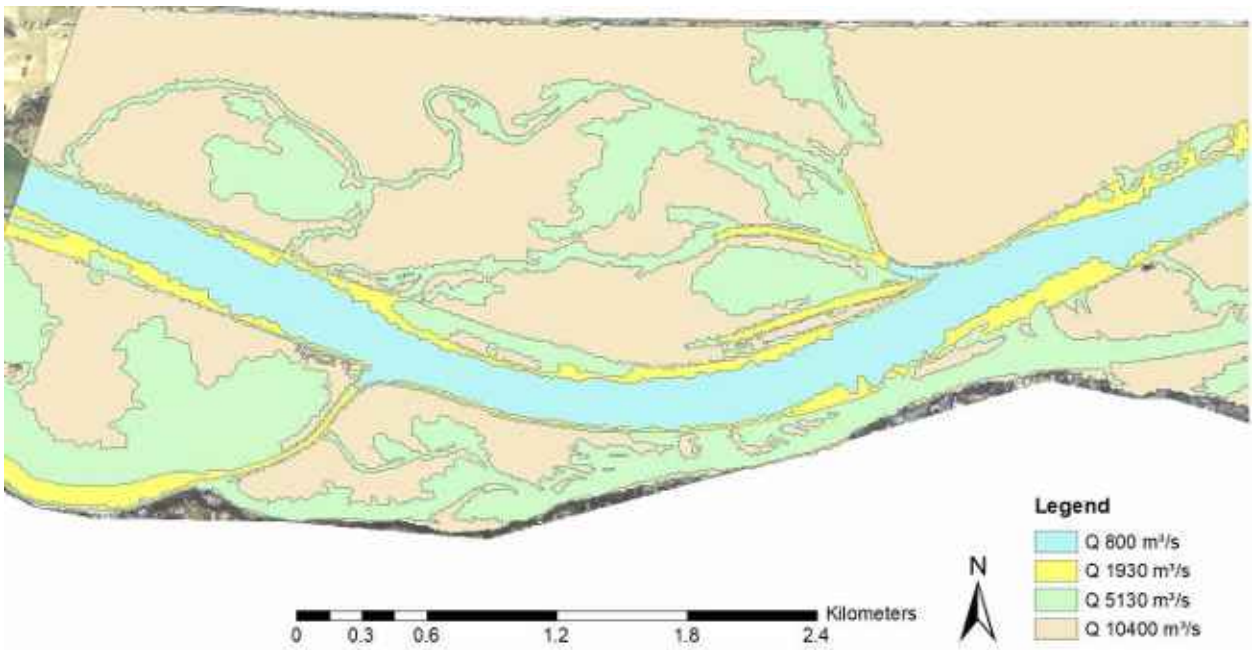


Figure 38 Detail map of water levels – 2D model Vienna-Bratislava – examples – blue: 800 m³/s, yellow: 1930 m³/s, green: 5130 m³/s, orange: 10400 m³/s

5.2.4. Bank-near accumulation zones

Linear bank near accumulations zones as depicted in Figure 39 left are frequently found during site visits and sampling campaigns on the shore line in the Nationalpark Donau-Auen, predominately in shallow areas of gravel banks. Hence, it is assumed, that these accumulations occur during most frequent occurring discharge levels. In order use the modelling results in combination with the hydrology of the Danube River in the project area, daily average discharge values from 1977 to 2015 at the gauging station Hainburg were statistically analysed.

The classification of discharge was performed monthly containing the calculated mean discharge as well as the 25% and 75% quartiles. The result is shown in Figure 39 right clearly indicating, that due to the hydrological regime the discharge ranges can be separated in periods, namely spring/summer and autumn/winter. Calculated discharge values for the two periods range between 1450 m^3/s – 2850 m^3/s for the spring/summer period and between 1000 m^3/s – 2000 m^3/s for the autumn/winter period respectively.

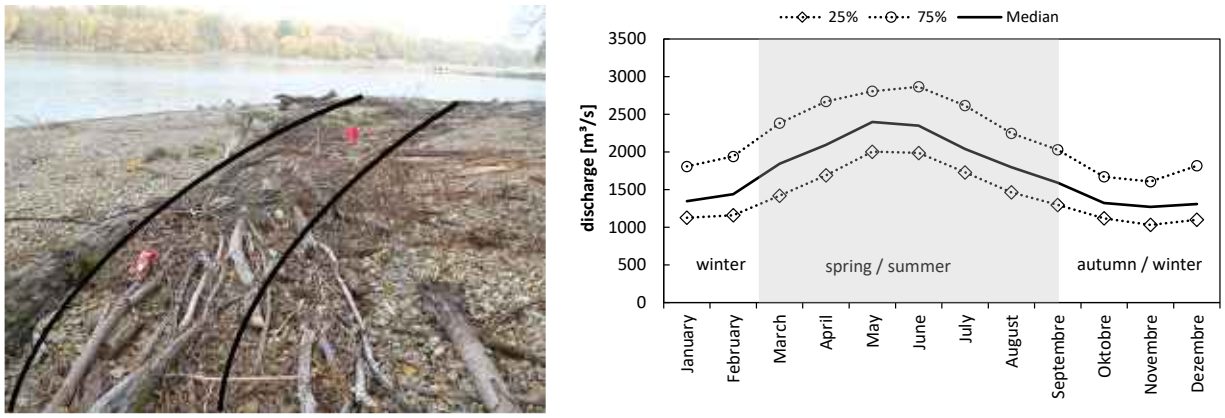


Figure 39 (left) bank near accumulation found during a site inspection near Haslau, right (statistical analysis of daily average discharge data at the gauging station Hainburg between 1977 - 2015

In a further step the water level maps from numerical simulations were used to identify and quantify areas of high accumulation potential on a seasonal basis. Giving a first insight and a rough estimate of potential areas in the project reach, the result for the section near Haslau are depicted in Figure 40 exemplarily.

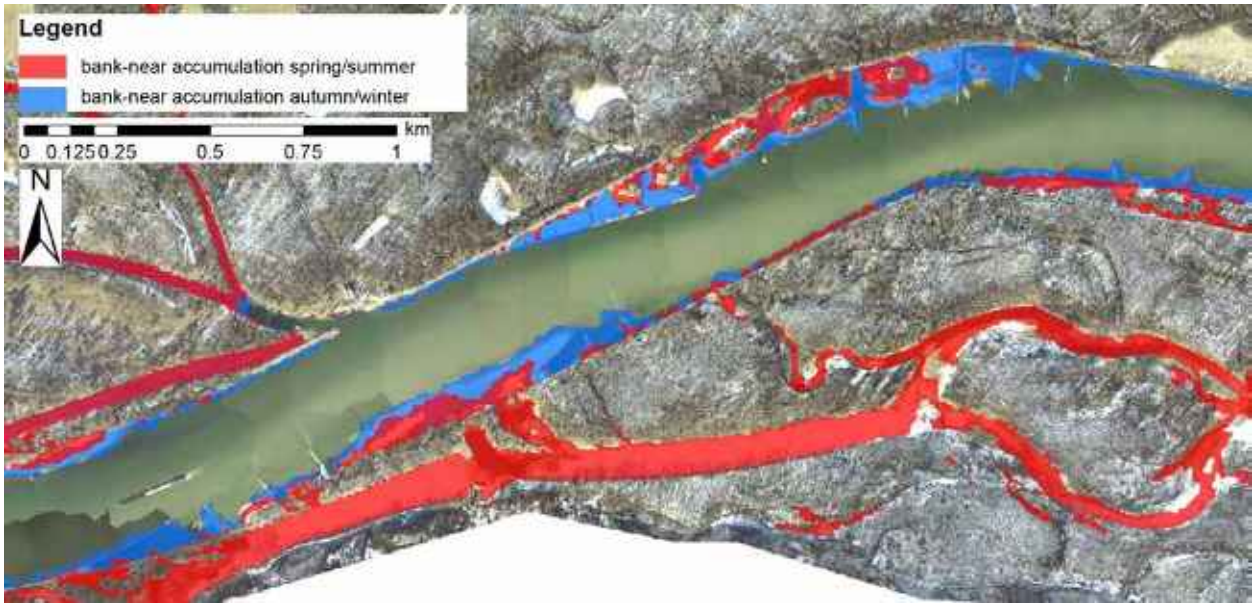


Figure 40 derived bank near accumulation zones for two periods - red: spring/summer (1450 m³/s - 2850 m³/s), blue: autumn/winter (1000 m³/s - 2000 m³/s)

For a more detailed evaluation and especially a quantification of macro plastic accumulation potential, conducted data of bank near sampling activities was combined with hydrological and numerical data as described in chapter 4.5.1. The hydrological discretisation for the reference gauging station Hainburg is presented in Figure 41. The graph indicates the maximum discharge within the period as well as the sampling date. Green sections in the timeline were determined as periods with descending water levels, excluding remobilisation between smaller discharge peeks.

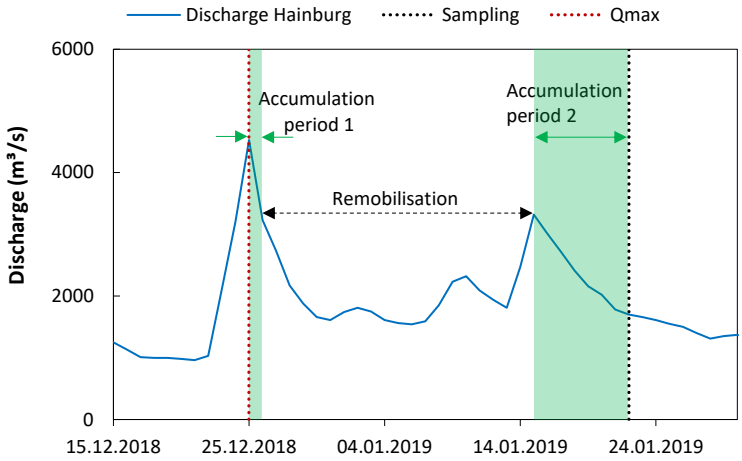


Figure 41 Determination of days with descending water level between two bank-near macro plastic samplings

Based on the hydrological analysis water level maps from the 2D numerical model Vienna-Bratislava were used to identify the areas of potential macro plastic accumulation within each sampling period. Distances between each sampling site as well as distances between maximum water level and water level of the sampling day at each sampling site were calculated as described in chapter 4.5.1. Based on this information, calculations of concentrations for the investigated reach as well as extrapolations for the whole project reach were elaborated. Generally, the calculated concentrations at the sampling sites ranged between 0.0 g/m² and 20.0 g/m² with an average value of

2.3 g/m². A visualisation of the determined areas for calculations towards macro plastic accumulation potential for sample 1 (22.01.2019) is given in Figure 42. The procedure was performed for 11 sampling dates covering a timeframe of almost 2 years.

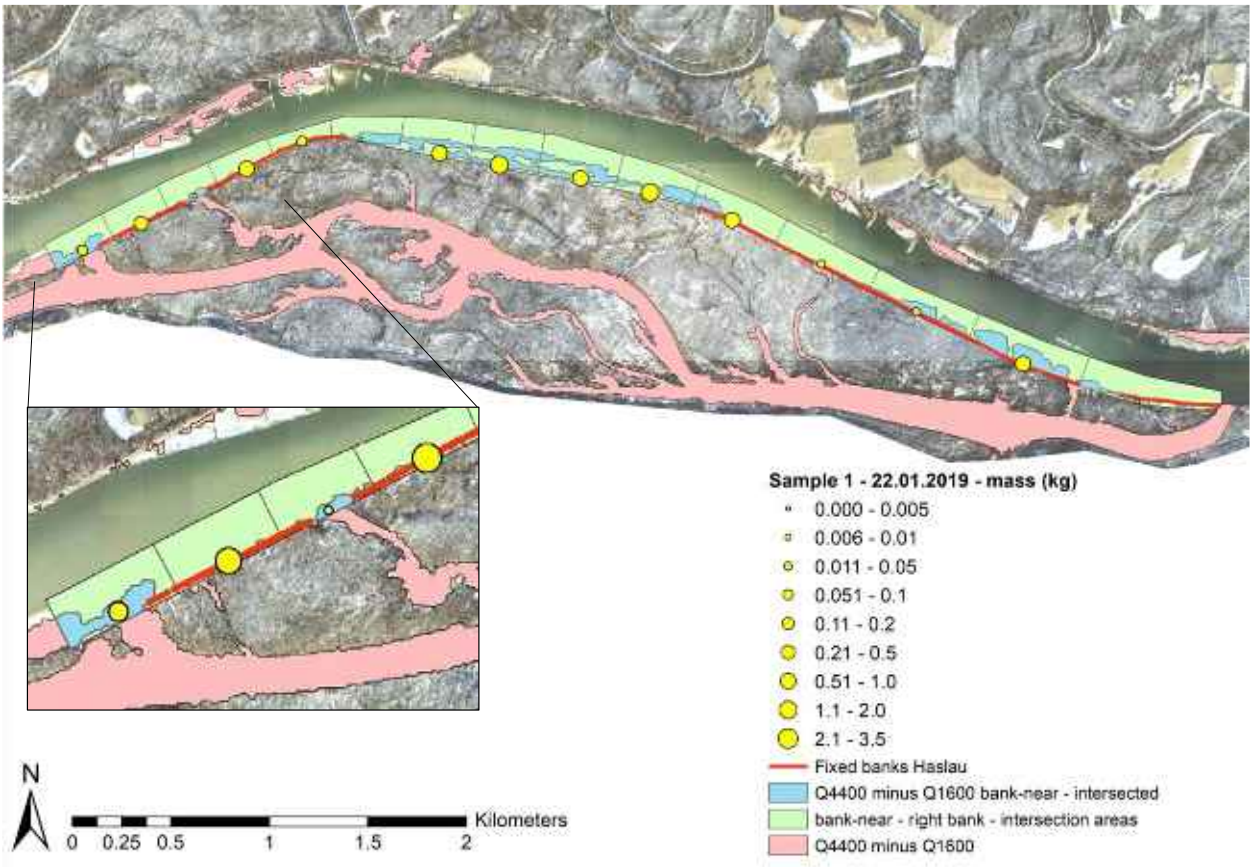


Figure 42 Determined areas for calculations towards macro plastic accumulation potential for sample 1 - 22.01.2019

An overview of determined hydrological and hydraulic parameters for all bank-near sampling periods near Haslau-Regelsbrunn is provided in Table 5.

Table 5 Overview of determined hydrological and hydraulic parameters for all bank-near sampling periods near Haslau-Regelsbrunn

Start (sampling)	End (sampling)	Q_{min}	Q_m	Q_{max}	$Q_{sampling}$	Date Q_{max}	total time (d)	time since Q_{max} (d)	time descending water level (d)	Q_{min} model	Q_{max} model
16.12.2018	22.01.2019	962	1992	4530	1700	25.12.2018	37	28	8	1600	4400
22.01.2019	26.02.2019	1280	1571	2640	1890	23.02.2019	35	3	3	1930	2800
26.02.2019	27.03.2019	1860	2673	4350	2190	17.03.2019	29	10	10	2400	4400
27.03.2019	02.07.2019	1590	2620	5150	2210	30.05.2019	97	33	21	2400	5130
02.07.2019	12.09.2019	1270	1619	2940	1730	30.07.2019	72	44	6	1930	2800
12.09.2019	31.10.2019	896	1217	1870	1000	11.10.2019	49	20	20	1000	1930
31.10.2019	24.01.2020	914	1187	1940	1030	19.11.2019	85	66	29	1000	1930
24.01.2020	06.04.2020	927	1868	4940	1090	04.02.2020	73	62	29	1000	4800
06.04.2020	07.05.2020	1120	1369	1540	1520	02.05.2020	31	5	11	1600	1600
07.05.2020	15.07.2020	1180	1974	4160	1650	22.06.2020	69	23	6	1600	4000
15.07.2020	09.11.2020	1070	1898	5400	1590	05.08.2020	117	96	13	1600	5600

In order to be able to extrapolate determined bank-near accumulation potential as described, first the data set was analysed. Therefore in Figure 43 the sampled plastic masses were plotted against the distance between sampling and maximum water level. Short distances indicate steep fixed bank sections, long distances indicate shallow gravel banks. As the graph shows, there is no clear correlation between these parameters. Hence, no assumptions towards the accumulation potential in connection to the elevation gradient of the shore line can be made.

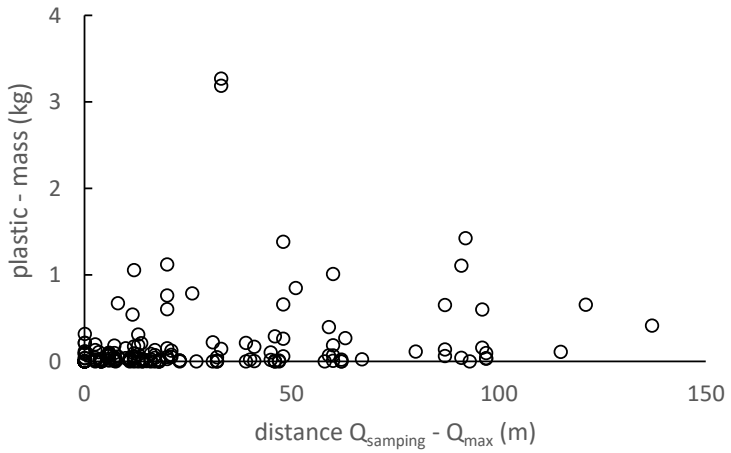


Figure 43 Relation between sampled plastic mass and the distance between sampling and maximum water level

Furthermore, the sampled section is considered as a representative section fort the Danube between Vienna and Bratislava, containing an inner and outer band situation, fixed banks as well as near natural shore lines, groyne fields and a related side channel system. Based on these findings, the calculated concentrations were used for temporal and spatial extrapolations of the macro plastic accumulation potential. Table 6 provides data contains data of macro plastic accumulation potential based on sampling periods ranging between 40.9 kg and 808.1 kg as well as per descending day ranging between 1.4 kg and 112.1 kg for the section Haslau-Regeslbrunn depending on the used method. By applying median and average values of the single periods, first masses per day and kilometre were calculated. During the whole investigation period of 695 days, 423 days showed constant or descending water level. Considering the days with constant/descending water level and extrapolating the average and median values for the 48 km reach, finally an accumulation potential for bank-near accumulation for the whole section on an annual basis can be estimated.

Table 6 Calculation of macro plastic accumulation potential - bank near - mass (kg)

	Accumulation per sampling period (kg)			Accumulation per descending day (kg)		
Date	Estimation (average concentration)	Estimation (sub-area concentration)	Calculation 2D model	Estimation (average concentration)	Estimation (sub-area concentration)	Calculation 2D model
22.01.2019	535.0	510.6	808.8	66.9	63.8	101.1
26.02.2019	160.3	145.2	211.1	53.4	48.4	70.4
27.03.2019	82.4	74.5	93.6	8.2	7.4	9.4
02.07.2019	66.1	61.5	94.7	3.1	2.9	4.5
12.09.2019	610.2	672.7	454.1	101.7	112.1	75.7
31.10.2019	300.5	358.0	551.4	15.0	17.9	27.6
24.01.2020	40.9	46.6	72.8	1.4	1.6	2.5
06.04.2020	147.9	171.3	183.6	5.1	5.9	6.3
07.05.2020	108.4	121.8	119.2	9.9	11.1	10.8
15.07.2020	93.3	127.7	123.2	15.5	21.3	20.5
09.11.2020	610.3	737.6	746.6	46.9	56.7	57.4

	mass per descending day - sampling reach (6.3 km)		
Average	29.8	31.8	35.1
Median	15.0	17.9	20.5

	mass per descending day - per km		
Average	4.7	5.0	5.6
Median	2.4	2.8	3.3

	hydrological indicators - sampling duration		
Sampling period (d)	695	695	695
Descending water level (d)	423	423	423
Descending water level per year (d)	222	222	222

	mass per year and km		
Average	1 049	1 120	1 238
Median	530	631	724

	mass per year Vienna - Bratislava (48 km)		
Average	50 357	53 739	59 430
Median	25 434	30 297	34 743

The resulting graph showing macro plastic accumulation potential on the right bank of the Danube between Vienna and Bratislava is provided in Figure 44. The graph shows that the estimated amounts based on average values are much more sensitive to outliers than the ones based on the median values. In general, all three calculation methods leading to results in the same range of values between 25 and 60 t/a. This number represents an estimated **potential** accumulation during constant and descending water levels and is **not considering remobilisation processes**.

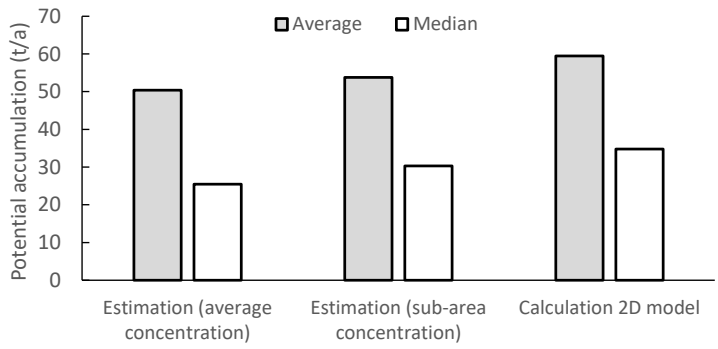


Figure 44 Annual macro plastic accumulation potential - bank-near - right bank - Vienna-Bratislava (48 km) – mass (t/a)

In the same way, the accumulation potential was calculated using input data related to particle numbers. The resulting graph showing macro plastic accumulation potential on the right bank of the Danube between Vienna and Bratislava for Mio. Pieces is provided in Figure 45. Depending on the calculation methods, the estimations leading to results ranging between 4.6 and 7.8 Mio. pieces/a. This number represents an estimated potential accumulation during constant and descending water levels and is not considering remobilisation processes.

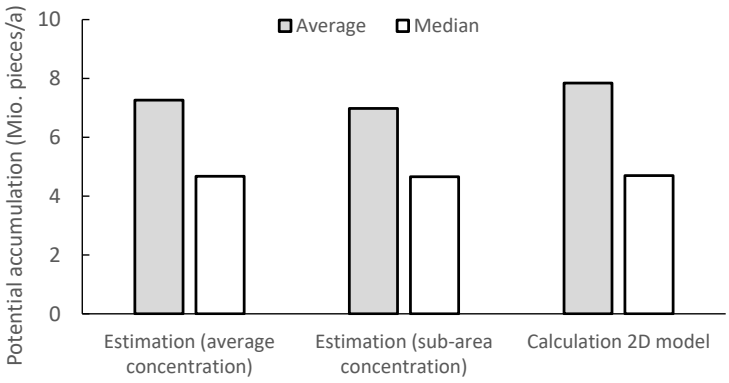


Figure 45 Annual macro plastic accumulation potential - bank-near - right bank - Vienna-Bratislava (48 km) – particle numbers (Mio. pieces/a)

This means, that specific plastic items may appear several times in the analysis if they are remobilized and then stranded again. The parameter therefore **does not directly show a plastic quantity but rather represents as a potential** to show the proportion of plastic, that could be extracted from the system.

5.2.5. Floodplain accumulation

Results from the macro plastic samplings in the floodplain in terms of concentration (kg/m²) are depicted in Figure 46 for the sampling of 06.04.2020 and in Figure 47 for the sampling of 17.12.2020. Besides the concentration the specific discharge as a product of flow velocity and water depth for the discharge of 6000 m³/s is displayed. A comparison of the 2 sampling dates reveals areas with high concentrations for both samplings, e.g. in inflow areas to the side channel system). Besides it was found, that in sampling sites above the submerged area, only plastic was found at the first sampling date, leading to the assumption that the found macro plastic must be from former discharge events.



Figure 46 Macro plastic sampling in the floodplain - 06.04.2020 – concentrations (white circles) and specific discharge for Q6000 of the flooded area in the Haslau-Regelsbrunn side channel system



Figure 47 Macro plastic sampling in the floodplain – 17.12.2020 – concentrations (white circles) and specific discharge for Q6000 of the flooded area in the Haslau-Regelsbrunn side channel system

An analysis plotting different hydraulic parameters against measured concentrations of micro plastic was performed based on samplings and model results as shown in Figure 48. As data shows, no clear relation between accumulation data and hydraulic parameters like water depth, flow velocities and specific discharge can be drawn leading to the assumption, that deposition processes in this area are highly influenced by filtering effects of vegetation.

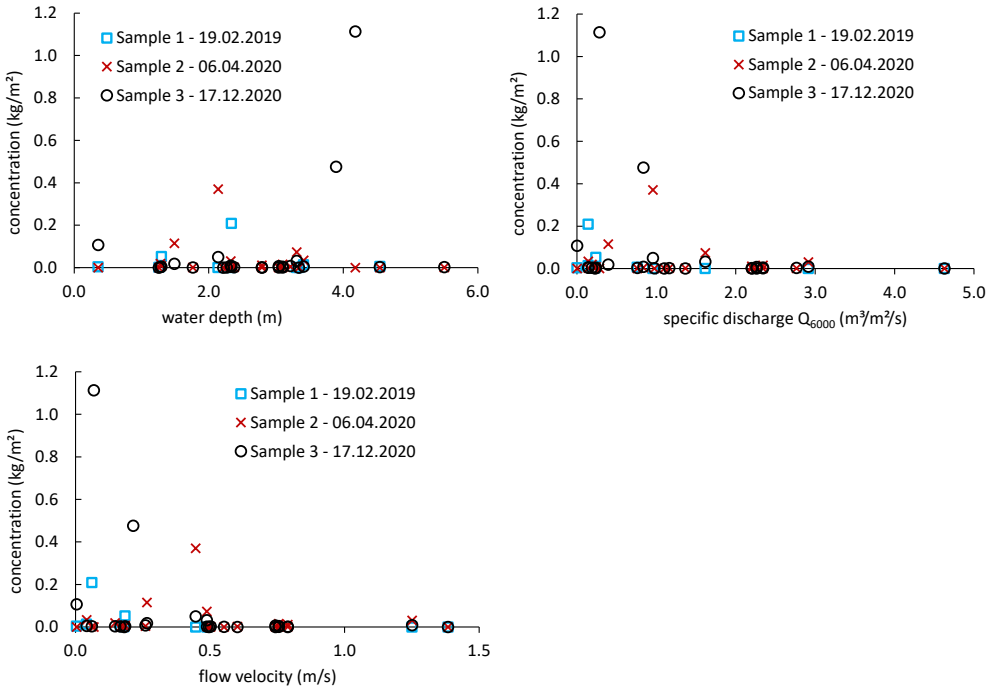


Figure 48 Analysis of hydraulic parameters in relation to macro plastic concentration – Haslau-Regelsbrunn - upper left: water depth, upper right: specific discharge, lower left: flow velocity

Figure 49 and Figure 50 comprise a closer look towards areas of accumulation in the side channel system. In Figure 49 areas of flow diversion from the Danube into the side channel system are depicted, clearly indicating high accumulation potential in these areas. In these sections, where plastic enters the side channel, high amounts of plastic deposit, often related to dense vegetation found in the floodplain area. Accumulations were moreover found at various spots with woody debris as shown in Figure 50. These often-found characteristic elements of side channel systems build a natural barrier for macro plastic entering the floodplain.



Figure 49 Macro plastic accumulations in the inflow sections to the side channel system Haslau-Regelsbrunn

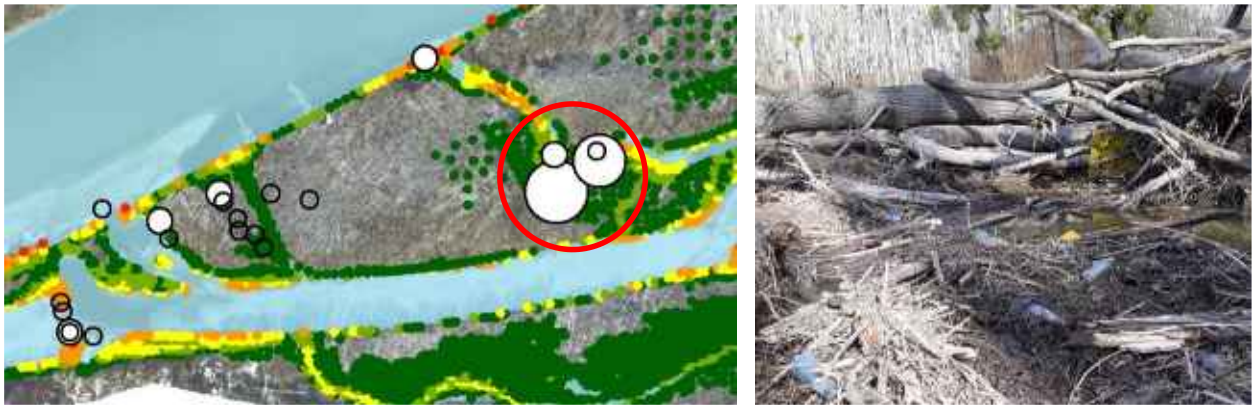


Figure 50 Macro plastic accumulations related to woody debris in the side channel system Haslau-Regelsbrunn

Generally, the sampling actions in the side channel systems were more focussed on accumulation hotspots than in the bank-near samplings. However, maximum concentrations of 1130 g/m² compared with bank-near maximum concentration of 20 g/m² indicate, that the floodplain area works as a filter due to its vegetation.

In order to evaluate the frequency and quantity of connection to the main channel, water flow into the side channels were analysed. Therefore, results from the 2D numerical model were evaluated for several discharges between 2400 m³/S and 6000 m³/s. The four investigated side channel systems and the related water levels at 2400 m³/S and 6000 m³/s are depicted in Figure 51.

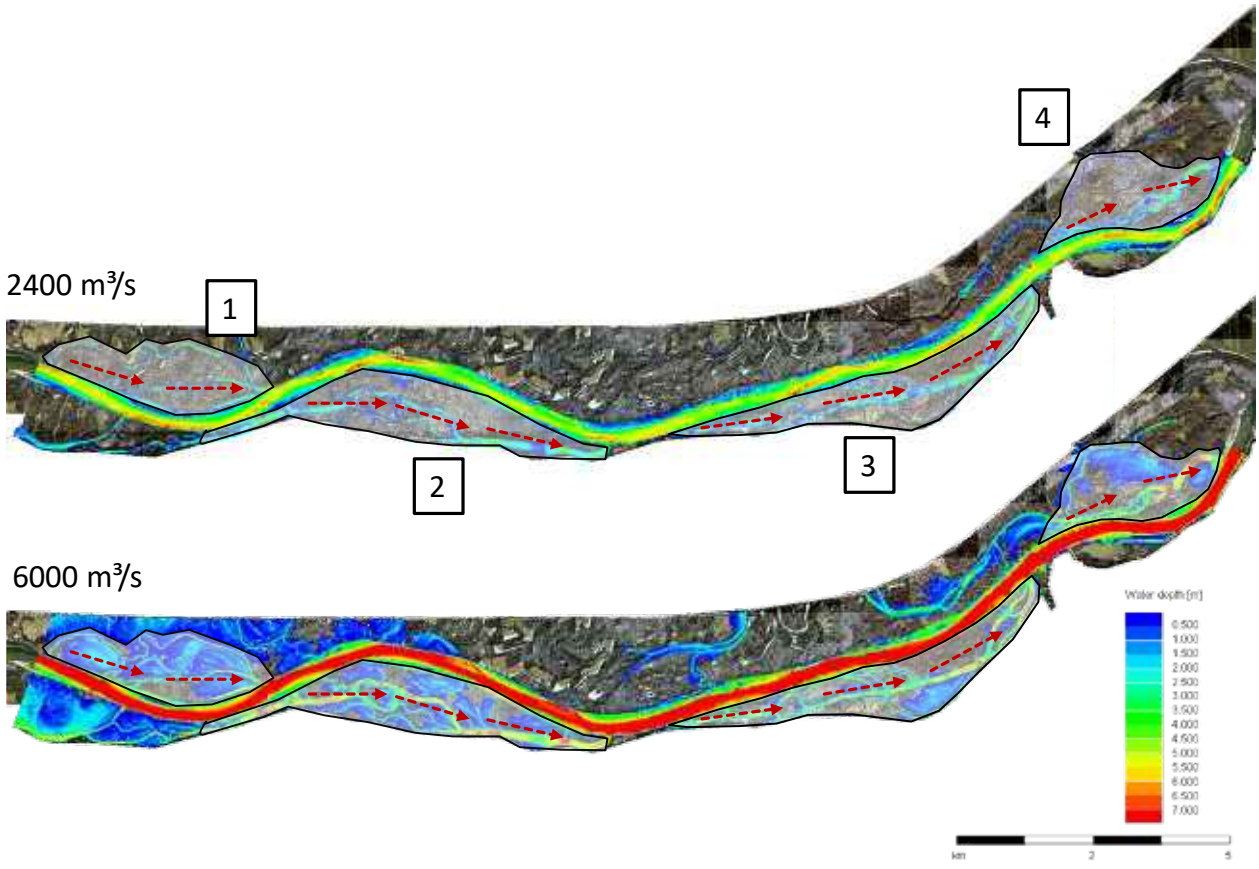


Figure 51 Water level maps and delineation of side channel systems in the 2D model Vienna – Bratislava for 2400 m³/s and 6000 m³/s

As shown in the graphs in Figure 52, the dotation of the side channel systems mostly starts around 2000 m³/s to 2400 m³/s except for side channel system3. At 6000 m³/s the amount of water diverted into the single side channels ranges between 2.3 % and 5.7 %, leading to a sum of almost 16 % of water diverted from the main channel of the Danube River in this section.

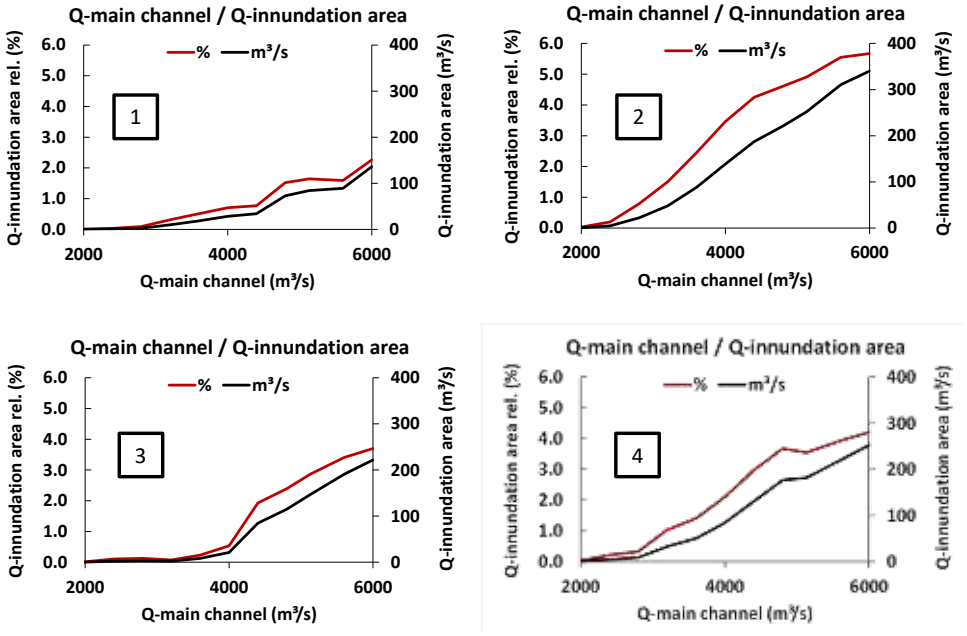


Figure 52 Quantification of discharges in the side channel systems depending on modelled discharges

Regarding the hydrological time series of Danube discharges between 1977 and 2015, flows between 2400 m³/s and 6000 m³/s occur during 0.4 % and 22.7 % of the days. However, with respect to the discharge regime this means that during this percentage of days discharge quantities between 1.4 % and 36.9 % are recognized (Figure 53). Generally, this means that high discharges occur rarely. However, with higher discharges macro plastic concentration is rising due to remobilisation processes and overflow at hydropower plants (as indicated in Figure 53), additionally more water is diverted into the side channels leading to high accumulation potential in combination with filtering processes due to vegetation.

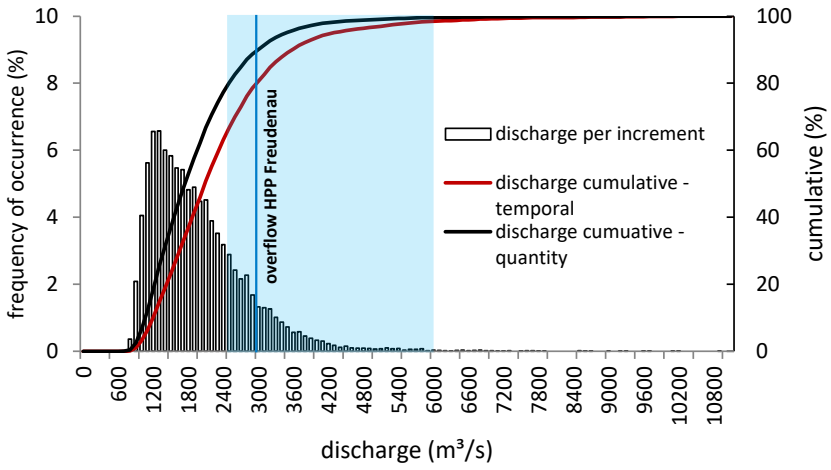


Figure 53 Classified and cumulative discharge for the Danube (Hainburg) - 1977 - 2015

6. Summary and Conclusiones

Within activity 3.6 "3D hydrodynamic modelling of selected plastic accumulation zones" it was aimed to describe fluvial processes related to plastic waste in river systems by the means of numerical simulation. Therefore following models with different approaches were built up in order to improve process understanding of macro plastic transport in the Danube River east of Vienna:

- 3D model Haslau-Regelsbrunn: River-kilometer 1901 - 1903,5
- 3D model Haslau-Wildungsmauer-Witzelsdorf: River-kilometer 1903,5 1891,7 - 1895,2
- 2D model Vienna-Bratislava: River-kilometer 1907 - 1881,3
- 3D concept model

The resulting 2D and 3D information of flow velocities and flow directions, bed shear stresses, partial flows and water level positions for different discharge conditions were used for further analysis. Besides the analysis performed within this task, the results build the basis for deliverable "D.3.7.1 Parameters and indicators for plastic accumulation processes".

Within this activity, the results were mainly used to describe and quantify accumulation processes in bank-near and floodplain area. Calculations towards the accumulation potential were derived combining systematic repetitive samplings of macro plastic, hydrological data and numerical modelling results. Following findings can be concluded from the investigations:

<u>Bank- near accumulation:</u>

- Classification of long-term discharge data on a monthly basis reveal, that due to the hydrological regime the discharge of the Danube River can be separated in periods, namely spring/summer (1450 m^3/s – 2850 m^3/s) and autumn/winter (1000 m^3/s – 2000 m^3/s). Using numerical model results, the areas between these discharge levels can be detected. During these most frequent occurring discharge levels plastic accumulates on the banks, as often found during sampling campaigns
- A methodology for upscaling of bank-near macro plastic sampling data on the project reach scale was developed. Assuming the sampled area as representative (containing an inner and outer band situation, fixed banks as well as near natural shore lines, groyne fields and a related side channel system) and that plastic accumulated only during declining discharges, an accumulation potential ranging between 25 to 60 t/a or 4.6 to 7.8 Mio. pieces/a for the right river bank of the Danube was estimated. The calculated concentrations at the sampling sites ranged between 0.0 g/m^2 and 20.0 g/m^2 with an average value of 2.3 g/m^2. As specific plastic items may appear several times in the analysis, if they are remobilized and then stranded again. The parameter therefore does not directly show a plastic quantity but rather represents a potential to show the proportion of plastic, that could be extracted from the system.

<u>Floodplain accumulation:</u>

- No clear relation between accumulation data and hydraulic parameters like water depth, flow velocities and specific discharge can be drawn.
- Accumulation processes, however, were found to have a clear correlation to vegetation and woody debris leading to high macro plastic concentrations. Maximum concentrations of 1130 g/m^2 compared with bank-near maximum concentration of 20 g/m^2 indicate, that the floodplain area works as a filter due to its vegetation.

- Quantification of partial discharges in the side channel systems show, that flood events and the related remobilisation of plastics in combination with overtopping of the hydro power plant Freudenau are a main factor for floodplain accumulation.

7. Directories

7.1. List of figures

Figure 1 Defined modelling reaches for 2D and 3D numerical simulation based on accumulation zones detected during site visits, expertise from Nationalpark Donau-Auen and GIS-bases analysis of the hydraulic structures of the Danube River 4
Figure 2 Model reach - 3D numerical model – Haslau-Regelsbrunn 5
Figure 3 Model reach - 3D numerical model – Wildungsmauer-Witzelsdorf 6
Figure 4 Model reach - 2D numerical model – Vienna-Bratislava 7
Figure 5 Construction methods and associated flow patterns of groynes (Patt et al., 2011) 8
Figure 6 Vortex formation in groyne field as a function of geometry (Sukhodolov et al., 2002) 9
Figure 7 Velocity distribution and vortex formation during flow around a groyne (Schnauder et al., 2015) 9
Figure 8 Near-surface velocity vectors during overflow of a groyne (Schnauder et al., 2015) 10
Figure 9 Digital Terrain Models – (a) Vienna-Bratislava, (b) Haslau-Regelsbrunn and (c) Wildungsmauer-Witzelsdorf 15
Figure 10 Terrain data analysis and resulting digital terrain models for the concept model - mode1: plane bed; model 2: inner and outer bed sequences 16
Figure 11 Concept model with integrated groynes - mode1: plane bed; model 2: inner and outer bed sequences 16
Figure 12 Computational mesh - 3D model Haslau-Regelsbrunn 17
Figure 13 Cell sizes - computational mesh - 3D model Haslau-Regelsbrunn 18
Figure 14 Computational meh for the 2D model - Vienna-Bratislava 18
Figure 15 Strickler values for the 2D model Vienna-Bratislava 20
Figure 16 Overview of performed ADCP (red) and water level (orange) measurements at the Danube east of Vienna 21
Figure 17 Results of the GPS water level measurement - red: Q1950 m³/s, black: Q 910 m³/s 21
Figure 18 Results of the ADCP flow velocity and discharge measurement – upper graph: Q890 m³/s, lower graph: Q 1950 m³/s 22
Figure 19 Visualisation of the residuals for a convergent numerical solution 23
Figure 20 Visualisation of teh mass balance for a convergent numerical solution 23
Figure 21 (left) Hydrograph of daily average discharge values, (right) characteristic discharge values - gauging station Hainburg 24
Figure 22 Diagram of hydrograph (blue), bank near samplings BOKU (black), hinterland samplings BOKU (red) and Nationalpark samplings (green) conducted within the project period 24
Figure 23 Defined sampling points for repeated bank near and Hinterland sampling of macro plastic 25
Figure 24 Sketch of the methodology towards combination of sampling data with hydrological and numerical data to describe bank near accumulation potential 27
Figure 25 3D model Haslau-Regelsbrunn - flow velocity – top: RNQ 980 m³/s, centre: MQ 1930 m³/s, bottom: Q 3000 m³/s - surface near layer 29
Figure 26 3D model Haslau-Regelsbrunn – bed shear stress – top: RNQ 980 m³/s, centre: MQ 1930 m³/s, bottom: Q 3000 m³/s - surface near layer 30
Figure 27 3D model Haslau-Regelsbrunn – water level – top: RNQ 980 m³/s, centre: MQ 1930 m³/s, bottom: Q 3000 m³/s 32
Figure 28 3D model Wildungsmauer-Witzelsdorf - flow velocity – top: RNQ 980 m³/s, centre: MQ 1930 m³/s, bottom: Q 3000 m³/s - surface near layer 34
Figure 29 3D model Wildungsmauer-Witzelsdorf – water level – top: RNQ 980 m³/s, centre: MQ 1930 m³/s, bottom: Q 3000 m³/s 35

Figure 30 3D concept model – flow velocity – RNQ 980 m³/s – top: model 1, centre: model 2, bottom: difference plot (model 2 minus model 1) 36
Figure 31 3D concept model – flow velocity – Q 3000 m³/s – top: model 1, centre: model 2, bottom: difference plot (model 2 minus model 1) 37
Figure 32 3D concept model – flow velocity – MQ 1930 m³/s – top: model 2, bottom: model 3 38
Figure 33 3D concept model – water level – RNQ 980 m³/s – top: model 1, bottom: model 2 39
Figure 34 3D concept model – water level – Q 3000 m³/s – top: model 1, bottom: model 2 40
Figure 35 2D model Vienna-Bratislava – flow velocity – RNQ 980 m³/s, MQ 1930 m³/s, HSQ 5130 m³/s, HQ_{100} 10400 m³/s 41
Figure 36 2D model Vienna-Bratislava – water depth – RNQ 980 m³/s, MQ 1930 m³/s, HSQ 5130 m³/s, HQ100 10400 m³/s 42
Figure 37 Map of water levels – 2D model Vienna-Bratislava – examples – blue: 800 m³/s, yellow: 1930 m³/s, green: 5130 m³/s, orange: 10400 m³/s 43
Figure 38 Detail map of water levels – 2D model Vienna-Bratislava – examples – blue: 800 m³/s, yellow: 1930 m³/s, green: 5130 m³/s, orange: 10400 m³/s 43
Figure 39 (left) bank near accumulation found during a site inspection near Haslau, right (statistical analysis of daily average discharge data at the gauging station Hainburg between 1977 - 2015 44
Figure 40 derived bank near accumulation zones for two periods - red: spring/summer (1450 m³/s - 2850 m³/s), blue: autumn/winter (1000 m³/s - 2000 m³/s) 45
Figure 41 Determination of days with descending water level between two bank-near macro plastic samplings ... 45
Figure 42 Determined areas for calculations towards macro plastic accumulation potential for sample 1 - 22.01.2019 46
Figure 43 Relation between sampled plastic mass and the distance between sampling and maximum water level 47
Figure 44 Annual macro plastic accumulation potential - bank-near - right bank - Vienna-Bratislava (48 km) – mass (t/a) 48
Figure 45 Annual macro plastic accumulation potential - bank-near - right bank - Vienna-Bratislava (48 km) – particle numbers (Mio. pieces/a) 49
Figure 46 Macro plastic sampling in the floodplain - 06.04.2020 – concentrations (white circles) and specific discharge for Q6000 of the flooded area in the Haslau-Regelsbrunn side channel system 50
Figure 47 Macro plastic sampling in the floodplain – 17.12.2020 – concentrations (white circles) and specific discharge for Q6000 of the flooded area in the Haslau-Regelsbrunn side channel system 51
Figure 48 Analysis of hydraulic parameters in relation to macro plastic concentration – Haslau-Regelsbrunn - upper left: water depth, upper right: specific discharge, lower left: flow velocity 52
Figure 49 Macro plastic accumulations in the inflow sections to the side channel system Haslau-Regelsbrunn 52
Figure 50 Macro plastic accumulations related to woody debris in the side channel system Haslau-Regelsbrunn .. 53
Figure 51 Water level maps and delineation of side channel systems in the 2D model Vienna – Bratislava for 2400 m³/s and 6000 m³/s 53
Figure 52 Quantification of discharges in the side channel systems depending on modelled discharges 54
Figure 53 Classified and cumulative discharge for the Danube (Hainburg) - 1977 - 2015 54

7.2. List of tables

Table 1 Overview of used cell sizes for the developed 3D numerical models 18
Table 2 Overview of used cell sizes for the developed 2D numerical model 18
Table 3 Bank near macro plastic sampling (BOKU) – mass (kg) 25
Table 4 Bank near macro plastic sampling (BOKU) – number of pieces 26
Table 5 Overview of determined hydrological and hydraulic parameters for all bank-near sampling periods near Haslau-Regelsbrunn 46

Table 6 Calculation of macro plastic accumulation potential - bank near - mass (kg)..... 48

8. References

Andrady, A. (2011): Microplastics in the marine environment. Marine Pollution Bulletin 62 (2011), 1596 – 1605.

Arthur, C; Baker, J; Bamford, H (2008): Proceedings of the International Research Workshop on the Occurrence, Effects and Fate of Microplastic Marine Debris. Sept 9−11; NOAA Technical; Memorandum NOS-OR&R-30, 2009.

BMLFUW / ÖWAV (2011): Fließgewässermodellierung - Arbeitsbehelf Feststofftransport und Gewässermorphologie. Bundesministerium für Land- und Forstwirtschaft, Umwelt und Wasserwirtschaft; Österreichischer Wasser- und Abfallwirtschaftsverband (Hrsg.), Wien.

Breitbarth M. (2017): Abfälle in deutschen Fließgewässern: Eintrags- und Austragspfade, Zusammensetzungen, Aufkommen und Vermeidungsmaßnahmen. Schriftenreihe des Fachgebietes Abfalltechnik, Universität Kassel. Band 22.

Browne, M; Galloway, T; Thompson, R (2007): Microplastics – an emerging contaminant of potential concern? Integrated Environmental Assessment and Management 3: 559–561.

Fahrmeir L., Kneib T., Lang S. (2009): Regression Modelle, Methoden und Anwendungen, Zweite Auflage, Springer-Verlag Berlin Heidelberg 2007, 2009

Forkel, C. (2004): Numerische Modelle für die Wasserbaupraxis: Grundlagen, Anwendungen, Qualitätsaspekte, Mitteilungen des Lehrstuhls und Instituts für Wasserbau und Wasserwirtschaft der RWTH Aachen, Shaker Verlag.

GESAMP (2015): Sources, fate and effects of microplastics in the marine environment: a global assessment. GESAMP Report and Studies No. 90, International Maritime Organization - London, UK (2015), 96 S.

Giesecke, J., Heimerl, S. (2014): Wasserkraftanlagen. Planung, Bau und Betrieb. 6., aktualisierte u. erw. Aufl., Springer Vieweg, Berlin, Heidelberg.

Glas, M., Glock, K., Tritthart, M., Liedermann, M., Habersack, H. (2018): Hydrodynamic and morphodynamic sensitivity of a river's main channel to groyne geometry. Journal of Hydraulic Research (in Druck).

Glock, K. (2018): persönliche Mitteilung, Institut für Wasserwirtschaft, Hydrologie und konstruktiven Wasserbau, Universität für Bodenkultur, Wien.

Harrison, J., Hoellein, T., Sapp, M., Tagg, A., Ju-Nam, Y., Ojeda, J. (2018): Microplastic-Associated Biofilms: A Comparison of Freshwater and Marine Environments. In Freshwater Microplastics; Wagner, M., Lambert, S., Eds.; Springer: Cham, Switzerland, 2018.

Heeb, J., Hoffelner, W. (2004): MGU Littering-Studie – Zwischenbericht. Programm für Mensch, Gesellschaft und Umwelt (MGU). Universität Basel.

Hohenblum, P. et. al. (2015): Plastik in der Donau – Untersuchung zum Vorkommen von Kunststoffe in der Donau in Österreich. Umweltbundesamt GmbH, Wien.

Kowalski, N., Reichardt, A.M., Waniek, J.J. (2016): Sinking rates of microplastics and potential implications of their alteration by physical, biological, and chemical factors. Mar. Pollut. Bull. 2016, 109, 310–319.

Liedermann, M., Gmeiner, P., Pessenlehner, S., Haimann, M., Hohenblum, P., & Habersack, H. (2018). A methodology for measuring microplastic transport in large or medium rivers. Water, 10(4), 414.

Long, M., Moriceau, B., Gallinari, M., Lambert, C., Huvet, A., Raffray, J., Soudant, P. (2015): Interactions between microplastics and phytoplankton aggregates: Impact on their respective fates. Mar. Chem. 2015, 175, 39–46.

Malcherek, A. (2014): Vorlesungsskriptum Numerische Methoden der Strömungsmechanik, Institut für Wasserwesen, Universität der Bundeswehr München.

Nachtnebel, H. P. (2008): Vorlesungsskriptum Konstruktiver Wasserbau und Flussgebietsmanagement, Institut für Wasserwirtschaft, Hydrologie und konstruktiven Wasserbau; Universität für Bodenkultur, Wien.

Nationalpark Donau-Auen (2018): personal communication

Patt, H., Jürging, P., Kraus, W. (2011): Naturnaher Wasserbau – Entwicklung und Gestaltung von Fließgewässern. 4. Auflage, Springer Verlag Berlin Heidelberg.

Schnauder, I., Rüther, N., Anlanger, C. (2015): Wasserbaukolloquium 2015: Feldexperimente und Messungen der Strömung um Buhnen. Dresdner Wasserbauliche Mittteilungen Heft 38, 396 – 404.

Strobl, T., Zunic, F. (2006): Wasserbau: Aktuelle Grundlagen - Neue Entwicklungen, Springer Verlag.

Sukhodolov, A., Uijttewaal, W. S., & Engelhardt, C. (2002). On the correspondence between morphological and hydrodynamical patterns of groyne fields. Earth Surface Processes and Landforms, 27(3), 289-305.

Tritthart, M. (2005): Three-Dimensional Numerical Modelling of Turbulent River Flow using Polyhedral Finite Volumes. Wiener Mitteilungen Wasser-Abwasser-Gewässer 193, 1–179.

Tritthart, M. (2006): Wasserbaukolloquium 2006: Strömungssimulation im Wasserbau. Dresdner Wasserbauliche Mitteilungen Heft 32, 193 - 200.

Tritthart, M., Liedermann, M., Habersack, H. (2009): Modelling spatio-temporal flow characteristic in groyne fields. River Research and Applications, 25 (1), 62-81.

Tritthart, M. (2017): Vorlesungsskriptum Computerunterstützte Gewässermodellierung, Institut für Wasserwirtschaft, Hydrologie und konstruktiven Wasserbau, Universität für Bodenkultur, Wien.

Tritthart, M., Glock, K. (2018): Interim Report – Project FloodFlux, WP 2: Hydrological modelling.

Tweehuysen, G. (2015): Results of riverine macroplastics sampling with the Waste Free Waters sampler.

Online sources:

Nationalpark Donau-Auen (2017), Homepage des Nationalparks Donau-Auen, Die Donau, Online im Internet, URL: https://www.donauauen.at/natur-wissenschaft/die-donau/ [12.12.17]

Stadt Wien (2018), Homepage der Stadt Wien, Online im Internet, URL: https://www.wien.gv.at/umwelt/kanal/kanalnetz/ [12.05.18]

via donau, (2017), Homepage der via donau, Donau östlich von Wien, Online im Internet, URL: http://www.viadonau.org/unternehmen/projektdatenbank/top-aktuell/httpwwwviadonauorgfgp/donau-oestlich-von-wien/ [12.12.17]